A dopaminergic memory circuit drives acute valence via multiple neurotransmitters

Farhan Mohammad [1, 5, *], Yishan Mai [1, *], Joses Ho [2], Xianyuan Zhang [3], Stanislav Ott [1], James Charles Stewart [2], & Adam Claridge-Chang [1, 2, 4, 6]

1. Program in Neuroscience and Behavioural Disorders, Duke-NUS Medical School, Singapore.
2. Institute for Molecular and Cell Biology, A*STAR, Singapore.
3. Department of Pharmacology, National University of Singapore, Singapore.
4. Department of Physiology, National University of Singapore, Singapore.
5. Division of Biological and Biomedical Sciences, College of Health & Life Sciences, Hamad Bin Khalifa University, Qatar.
6. Correspondence: claridge-chang.adam@duke-nus.edu.sg
* Equal contribution

Abstract

The brain must guide immediate responses to beneficial and harmful stimuli while simultaneously writing memories for future reference. Both immediate actions and reinforcement learning are instructed by dopamine. However, it is unknown how dopaminergic systems maintain coherence between these two reward functions. Optogenetic activation experiments showed that the dopamine neurons that inform olfactory memory in *Drosophila* have a distinct, parallel function driving attraction and aversion (valence). Olfactory-memory neurons were dispensable for valence. A broadly projecting set of dopaminergic cells had valence that was dependent on dopamine, glutamate, and octopamine. Similarly, a more restricted dopaminergic cluster with attractive valence was reliant on dopamine and glutamate. Opto-inhibition of this narrow subset revealed that behavior was influenced by pre-existing dopaminergic activity. Dopamine's acute effect on valence provides a mechanism by which a dopaminergic circuit can coherently write memories to influence future responses while guiding immediate actions.

Keywords

Motivation, Reward, Valence, Reinforcement, Locomotion, Synapse, Dopamine

Introduction

For an animal to survive and thrive, its brain must integrate sensory stimuli and internal signals to guide it toward benefits and away from harm. Some neural information has evolved to be innately instructive to behavior—for example, a sensory response to painful heat. Other information has no inherent evolutionary imperative *a priori*, but can acquire behavioral meaning through learning. A fundamental aspect of all brain states is their propensity to make an animal approach or avoid a stimulus, a property termed 'emotional valence' [1]. In humans, an emotional behavior like a facial expression of disgust is characterized as having negative valence, while a happy smile can be said to have positive valence. It has long been appreciated that such emotional behaviors have counterparts in all animals, including insects [1–3]. In the brain, emotional valence is partly governed by neuromodulators, soluble factors that modify neuronal excitability and synaptic dynamics through their action on metabotropic receptors [4]. Through these cellular effects, neuromodulators transform circuit dynamics, eliciting various motor outputs from a single network [5].

One particularly important neuromodulator is dopamine. In mammals, dopamine-releasing cells have been implicated in diverse processes that include motor function, motivation, associative learning and acute valence [6–8]. Many of these functions are conserved across animal species, including the experimentally-tractable vinegar fly, *Drosophila melanogaster.*

Dopamine's importance has mainly been examined in associative functions including olfactory conditioning [9–11], aversive learning [12,13], and memories formed within the mushroom body (MB) [9,10,13–17]. The synaptic fields of the MB are formed from the confluence of ~2000 odor-responsive sensory Kenyon cells (KCs), 34 mushroom-body output neurons (MBONs), and ~120 dopaminergic cells (DANs) [18]. Both DANs and KCs synapse with MBONs [19], which affect behavioral valence by influencing locomotion [20]. Changes in olfactory valence arise when DANs modulate KC→MBON synaptic strength via dopamine release [21–23], resulting in the assignment of negative or positive valence to an odor response when coincident events activate aversive or appetitive DANs, respectively [23].

In addition to its diverse roles in olfactory memory [9,11,12,14,24–34], dopamine in the MB has also been implicated in regulating various non-olfactory, non-memory behaviors in *Drosophila.* These include innate odor preference [35–37], visual learning [38], sleep and circadian rhythm [39,40], temperature preference [41], oviposition choice [42], courtship drive [43], wing-extension

during courtship [44], decision-making [45,46], visual-attention [47], maintenance of flight state [48], odor discrimination [49], sensitivity to odor cues [50,51], discrimination and reaction to novel space [52], as well as signaling satiety and hunger to control foraging behavior [53–55]. Other recent studies have shown that dopamine modulates sensory processing: dopamine release in the antennal lobe (the primary olfactory processing center in *Drosophila*) enhances odor discrimination [49]; and dopamine also regulates the activity of local inhibitory neurons in the antennal lobe, leading to increased activity in projection neurons and enhanced sensitivity to odor cues [50,51].

Notably, DANs have also recently been associated with an array of different valent stimuli and behavior. DANs in the protocerebral anterior medial (PAM) cluster, which drives appetitive associative olfactory learning [9,32], innately respond to positively valent odors and are associated with upwind orientation and approach in response to those odors [51,56–59]. They are also implicated in responses to sugars and food-seeking behaviors [50,57,58,60,61], place-preference tasks [62,63], and response to carbon dioxide in larvae [64]. However, these studies have almost exclusively examined the role of PAM DANs with respect to external stimuli. It is known that the MBONs, when activated with thermogenetic or optogenetic channels, can autonomously drive valent behavior—even in the absence of odorants, food, or other orienting sensory stimuli [20]. This phenomenon of MBON valence establishes that mushroom-body circuits are capable of driving non-associative, acute valence. As such, an important question goes unanswered: is DAN activity in isolation also capable of driving acute valence behavior? To our knowledge, only one other study has explored this question, demonstrating DAN-mediated acute valence, and finding this property to be heterogeneous across different contexts [65].

In the present study, we addressed this question using optogenetic experiments, in which freely moving flies bearing optogenetic constructs were allowed to approach or avoid artificial activation of genetically defined dopaminergic cells in the PAM cluster. We found that flies are attracted to or avoid select DAN activities, but are largely indifferent to others. Genetic lesions indicate that dopaminergic acute valence is independent of MB sensory and associative functions, suggesting that this behavior is distinct from learning and that PAM activity is capable of driving valence in the absence of external stimuli. In a broad driver, valence depends on dopamine, glutamate and octopamine; in the β-lobe DANs, valence depends on both dopamine and glutamate, establishing roles for co-transmitters. An optogenetic inhibition

experiment of the β-lobe DANs revealed that, even in a low-stimulus environment, pre-existing neural activity contributes to ongoing locomotor behavior.

Results

Mushroom-body dopamine neurons drive approach and avoidance

To investigate the role of dopamine on acute approach/avoidance behaviors, we generated transgenic flies expressing an optogenetic activator (Chrimson, henceforth 'Chr') [66] in the paired-anterior-medial dopaminergic neurons (PAM DANs) that project to the MB [9,10,67]. The flies were then analyzed in a light-dark choice assay (**Figure 1a**). The *R58E02* is a fusion of a flanking region of the *Dopamine transporter* (*DAT*) gene fused with *Gal4* [68,69]. This driver expresses in a large subset of the PAM DANs, and has fibers in a broad set of MB neuropil zones [9,10,30,31,60,70] (**Figure 1b, S1a, Movie S1**). Valence was calculated as an effect size calculated as the mean difference between optogenetic test flies and the corresponding controls, and displayed as effect-size curves [71]. Flies expressing the Chr opto-activator with the *R58E02* transgene were strongly attracted to light (**Figure 1e, Movie S2**). By contrast, another driver, *R15A04*, expressed in PAM DANs that send fibers to a more restricted set of MB zones [31,60,69] (**Figure 1c, S1b, Movie S3**). These *R15A04>Chr* flies tended to avoid the light at the highest illumination intensity (70 μM/mm^2, **Figure 1f**). Thus, while activation of the *R58E02* DANs drives strong positive valence, flies will avoid activation in the subset defined by *R15A04*.

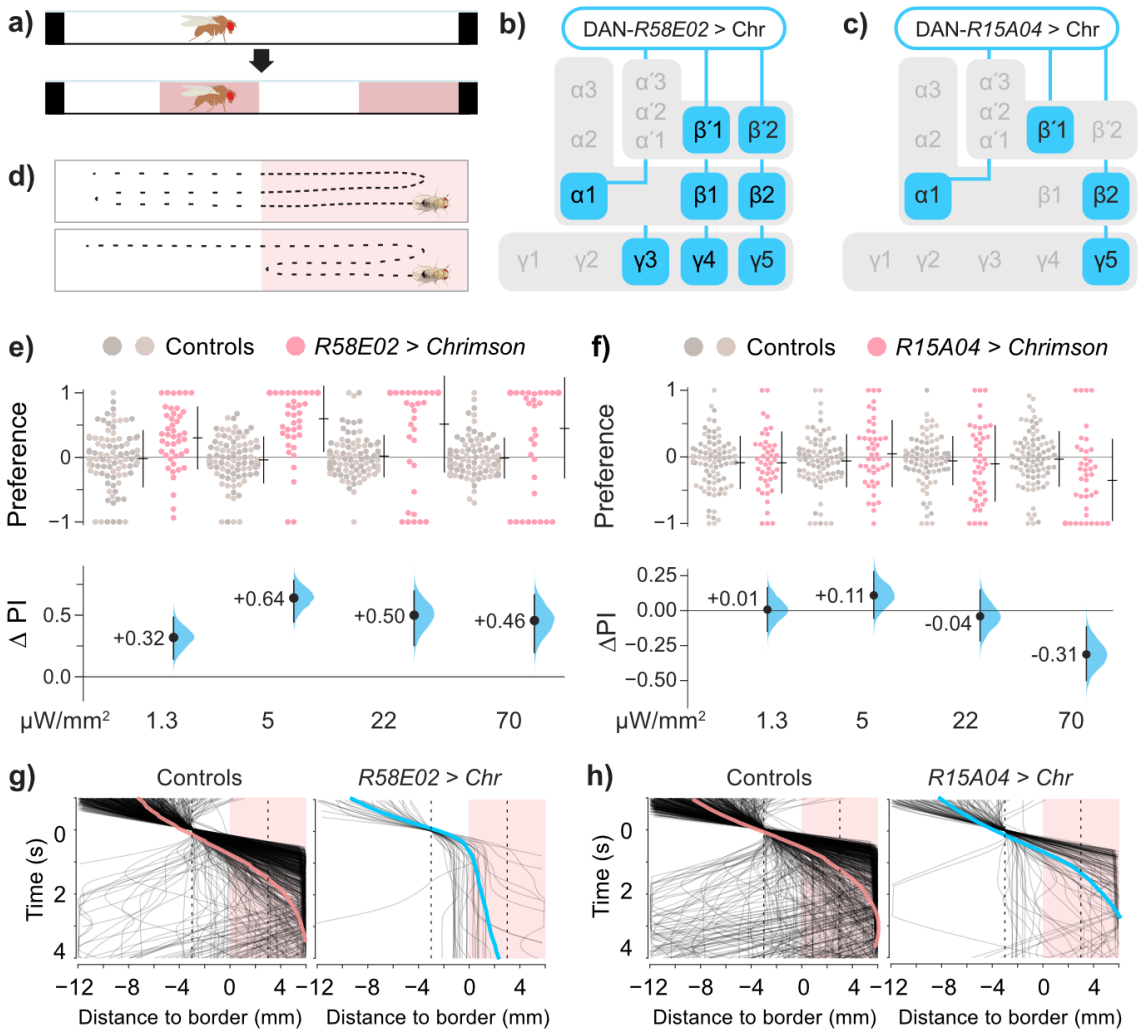

Figure 1. Activities in different dopaminergic cells drive valence

a. Optogenetic assay schematic showing that, after an initial dark phase, half of the chamber is illuminated with two bands of red light. See Methods for further details.

b–c. A schematic summary of two DAN drivers, *R58E02* and *R15A04*, with projections to MB synaptic zones. *R58E02* expresses in nearly all the PAM types, projecting to α1, β1, β2, β'1, β'2, γ4, and γ5, with weaker expression in γ1, γ2, and the peduncle. *R15A04* expresses in PAMs that project to the α1, β2, β'1, and γ5 zones.

d. Schematic of hypothetical locomotor modes for valence. **Top** Flies move slowly in the favored area. **Bottom** Flies maneuver to remain in the favored area. Either mode increases the time spent in the preferred area.

e. *R58E02>Chr* flies spent more time in the light zones. The **upper panel** shows the preference indices (PIs) for test flies (red dots) and driver and responder controls (*R58E02*/+ and *Chr*/+, gray dots). The **lower panel** shows the valence effect sizes (mean differences, ΔPI) between control and test flies, with confidence intervals

(black line) and the distribution of ΔPI error (blue curve). The positive ΔPI values indicate a positive valence. See **Table S1** for detailed genotypes and statistics.

f. *R15A04>Chr* flies avoided opto-activation. The negative ΔPI values indicate avoidance.

g. Walking behavior of the subset of flies that entered the choice zone from the dark side, as they approach the dark–light interface. Only data from flies that approached the choice zone were included. Traces of *R58E02>Chr* paths (black) are aligned to choice-zone entry, i.e. locked to the time of entering the boundary area. The colored lines show the overall mean trajectory. The horizontal axis is aligned to the middle of the choice zone. Test flies slowed or stopped at the boundary, with their heads on either side of the middle of the light interface.

h. Traces of *R15A04>Chr* flies as they enter the choice zone from the dark side. Trajectory data were taken from epochs with 70 μW/mm illumination.

DAN activation influences locomotion

When traversing a boundary between two stimulus areas, walking flies encountering aversive stimuli or an aversive odor use reversals or turns to maneuver away [14,20]. However, a fly displaying a spatial preference for one of two areas could hypothetically employ another locomotor mode: slowing down in the favored area (**Figure 1d**). We explored how valence, choice, and speed were associated in *R58E02* and *R15A04* flies. Regressions between preference, speed ratio, and a choice index showed that, in these lines preference was more strongly determined by differential speed (**Figure S1c-f**). We also inspected locomotion at the boundary by aligning the dark-to-light trajectories in a single experiment. In the subset of flies that entered the boundary choice-zone, trajectory lines drawn over time indicated that, as the optogenetic DAN lines traverse into the choice zone from the dark side, the *R58E02>Chr* flies tend to walk slower and frequently stop in the boundary area (**Figure 1g-h**). These observations suggest that these groups of DANs affect valence via walking-speed changes.

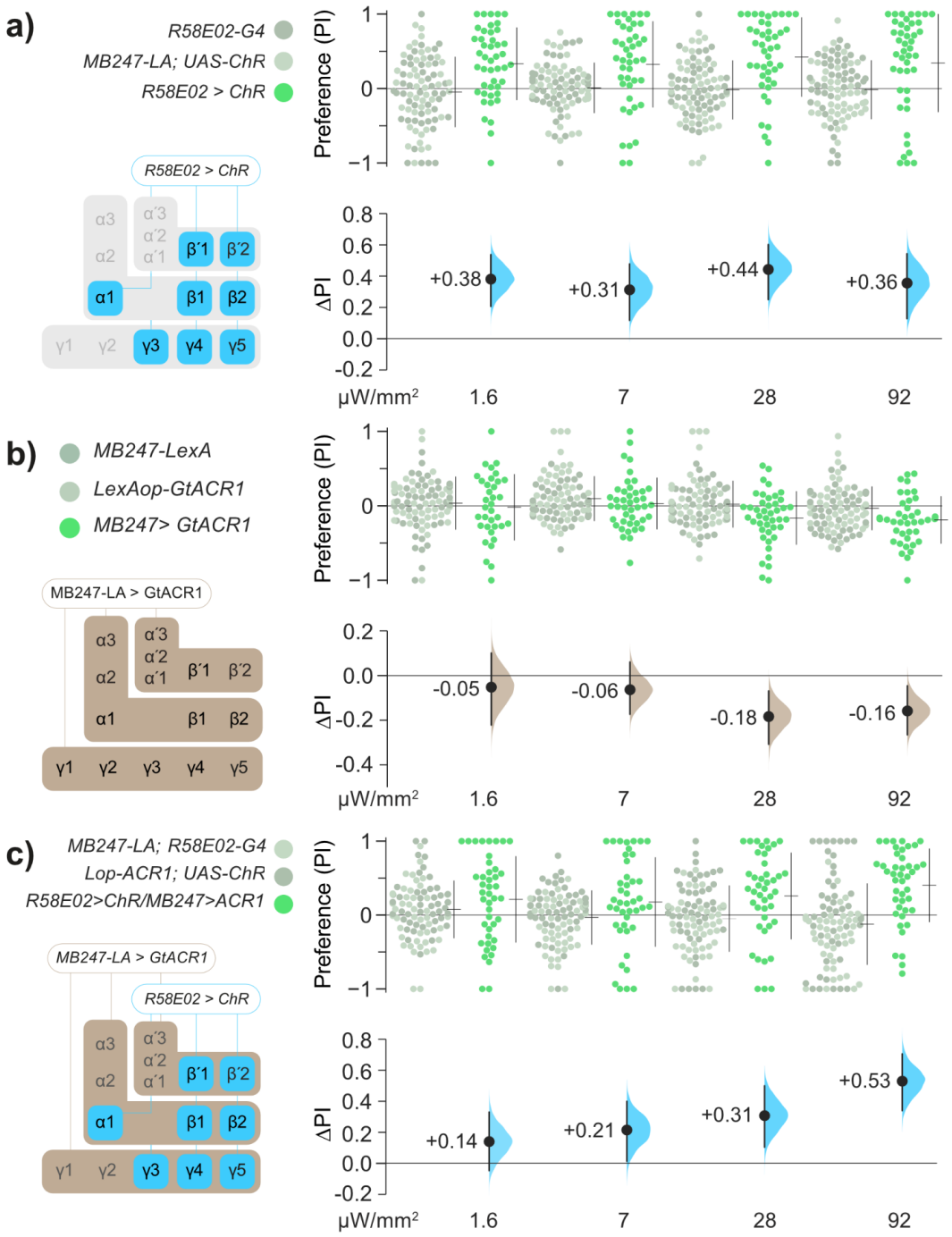

Figure 2. Kenyon cells are dispensable for *R58E02* DAN valence.

a. *R58E02>Chr* flies are attracted to green light. Left schematic illustrates the expression pattern of *R58E02*. Flies carrying all three transgenes displayed attraction to green light (green dots), resulting in positive valence (black dots and blue curves in the lower panel). Parental-type control flies (*R58E02-Gal4/+* or *MB247-LexA/+; UAS-Chr/+*, gray dots) showed a neutral preference for green light.

b. Relative to genetic controls, *MB247-LexA>lexAop-ACR1* flies display a modest avoidance of green light at high intensities (22 and 72 μW/mm^2). Schematic indicates that *MB247-LexA* drives expression of ACR in a majority of MB intrinsic Kenyon cells.

c. In *R58E02>Chr/MB247>ACR1* flies, preference for DAN activation mediated by *R58E02-Gal4>UAS-Chr* is unaffected by simultaneous opto-inhibition of the MB intrinsic cells with *MB247-LexA>lexAop-ACR1*. Effect sizes (blue curves) show the net effect of comparing test flies carrying all four transgenes (green dots) with controls (gray dots).

The Kenyon cells are dispensable for broad DAN attraction

DANs instruct odor memory by modulating KC function [21,23]. We thus asked whether, like memory, DAN optogenetic valence relies on KC activity [72,73]. We implemented a strategy to allow flies to simultaneously activate DANs with Chr and inhibit KCs using the light-actuated anion channelrhodopsin, GtACR1 (hereon 'ACR1') [74,75]. As both channelrhodopsins are responsive to green light, we tested the ability of green light to both activate DANs and silence KCs. *R58E02>Chr* flies were attracted to green light (**Figure 2a, S2a**), confirming effective Chr actuation. One possible confound would be if flies responded to KC inhibition with a strong attraction that masked DAN attraction; however, in a valence test, *MB247>ACR1* flies exhibited only mild aversion (**Figure 2b**). With aversive shock–odor conditioning under green light (**Figure S2e**), flies expressing the opto-inhibitor in the KCs (*MB247>ACR1*) failed to learn (**Figure S2f**), demonstrating that ACR1 sufficiently inhibits KCs to abolish memory formation. In *R58E02>Chr* flies, green light successfully induced optogenetic appetitive memories; however, in *R58E02>Chr, MB247>ACR1* flies, green light did not induce synthetic memory (**Figure S2g**), further verifying that ACR1 elicits KC inhibition. Flies carrying the *R58E02>Chr, MB247>ACR1* genotype were then tested for their optogenetic preference; even with inhibited KCs, valence remained intact (**Figure 2c, S2b**). Additional control experiments also showed that the olfactory receptor neurons are not required for PAM valence (**Figure S2c-d**). These results indicate that, for PAM-mediated attraction, olfactory input and KC activity are dispensable.

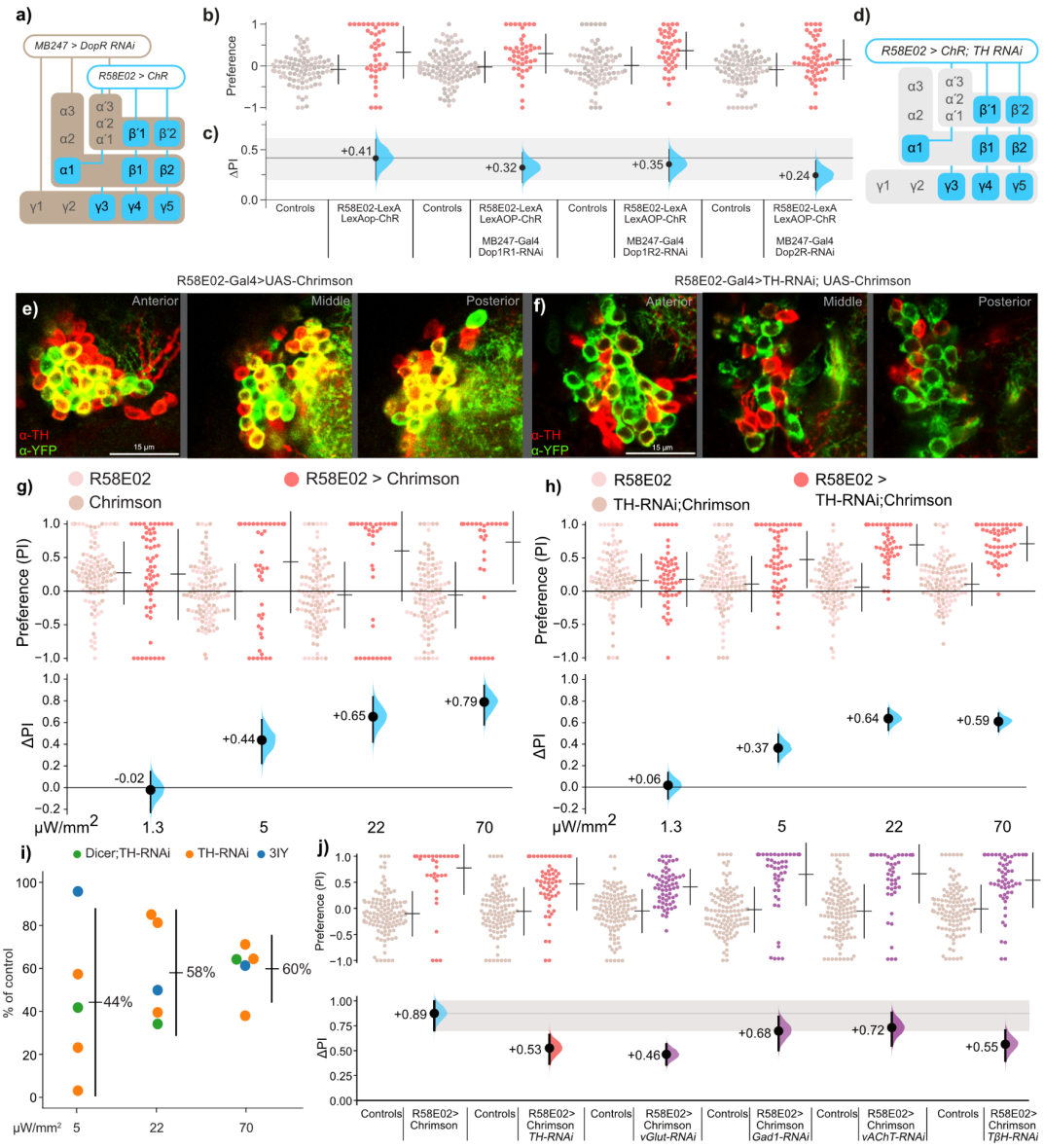

Figure 3. Dopamine is not unique in driving DAN-mediated attraction

a. Schematic illustrating the use of *MB247-Gal4* to use RNA interference to knock down receptor expression in the *R58E02-LexA>lexAop-Chr* optogenetic background.

b-c. Knocking down *Dop1R1*, *Dop1R2*, and *Dop2R* in the KCs had minor effects on *R58E02-LexA>lexAop-Chr* light attraction. The gray ribbon indicates the control-valence 95% confidence interval. Experiments used 72 µW/mm^2 red light.

d. Schematic for using *R58E02-Gal4* to simultaneously express Chrimson and knock down *TH* expression.

e. Immunohistochemistry of the PAM DAN cluster stained with α-TH (red) and α-YFP (green) in flies expressing Chr-YFP in the *R58E02* cells. Yellow rings indicate the co-localization of α-TH and α-YFP signals in cells in the PAM cell-body cluster at three optical slices.

f. Immunohistochemistry images of the DANs with TH-RNAi co-expression show that cells with α-YFP signal (*R58E02* cells) have a greatly lower α-TH signal.

g-h. Knocking down *TH* expression with TH-RNAi has a moderate effect on R58E02 valence across four intensities. For example, at 70 μW/mm^2 the valence is +0.79 ΔPI in *R58E02>Chr* flies (G) and is reduced to +0.59 ΔPI in flies carrying the *UAS-TH-RNAi* knockdown transgene (H).

i. Summary of the effects of reducing dopamine on *R58E02*-mediated valence with either gene knockdown (*UAS-TH-RNAi,* with or without *UAS-Dicer*) or a chemical inhibitor of TH activity (3-Iodo-L-tyrosine, 3IY). Each dot represents the percentage effect size of light intensity in an experiment (i.e., the *R58E02>Chr; TH-RNAi* experiment was replicated three times). Across all three intensities in five experiments, dopamine depletion resulted in an average ~46% reduction in valence. The vertical line indicates the 95% confidence interval.

j. A knockdown screen for neurotransmitters that contribute to *R58E02* valence. *R58E02>Chr* flies were crossed with RNAi transgenes targeting factors required for five transmitters: *TH* (dopamine, replicating the prior experiment), *vGlut* (glutamate), *GAD1* (GABA), *vAchT* (acetylcholine), and *TβH* (octopamine). The *vGlut* and *TβH* knockdowns showed a reduction in valence comparable to the *TH* knockdown.

Dopamine receptors in the KCs are dispensable to broad DAN attraction

For olfactory learning, dopamine receptor expression in the KCs is required [23,25,76]. To determine if this is also true for *R58E02* attraction, we knocked down the receptors *Dop1R1, Dop1R2,* and *Dop2R* in the KCs with RNAi transgenes [77]. For this, we used *R58E02-LexA* to drive *LexAop-Chr,* which, compared to *R58E02-Gal4*, yielded a relatively lower valence score. Individual knockdowns of all three receptors caused relatively minor reductions in valence (**Figure 3a-c**). This is consistent with the idea that *R58E02* valence is distinct from appetitive learning and that the KCs are not essential to *R58E02*-mediated valence.

Dopamine plays a partial role in *R58E02* valence

We aimed to estimate the extent to which *R58E02* valence has a requirement for dopamine. We depleted dopamine in the DANs with several methods. First, we used RNAi against tyrosine hydroxylase (TH), an essential enzyme for dopamine synthesis [78], encoded in flies by the *TH* gene (also referred to as *pale*). In *R58E02 > TH-RNAi* flies, immunohistochemical staining of the DANs showed that TH expression was markedly reduced (**Figure 3d-f, Movie S4-S5**). Compared to flies with intact TH expression (**Figure 3g**), flies with reduced TH in the *R58E02* DANs expressed substantially lower valence (**Figure 3h**). This partial valence reduction was observed in the three higher light intensities, and across three replications of this experiment (**Figure 3g-h, S3a-d**). We aimed to increase the RNAi transgene's efficacy with the simultaneous overexpression of Dicer2 endonuclease; this resulted in overall valence that was comparable to the RNAi alone (**Figure S3e, 3i**). Finally, we systemically depleted dopamine by feeding flies 3-iodotyrosine (3-IY), a competitive inhibitor of TH [79,80]. This pharmacological intervention also resulted in *R58E02>Chr* valence undergoing

a large partial reduction (**Figure S3f-g**). Averaging the results of all three interventions (*TH-RNAi* alone, *TH-RNAi* with *Dicer2*, and 3-IY) across three light intensities indicated that dopamine depletion reduces *R58E02*-mediated valence to 54% of control levels, i.e., an overall reduction of –46% (**Figure 3i**). So it appears that dopamine is mediating about half of *R58E02* valence.

Broad DAN attraction relies on glutamate and octopamine

Single-cell RNA sequencing data has shown that the PAMs express neurotransmitter-related genes aside from those pertaining to dopamine [34]. Since dopamine did not fully account for *R58E02* valence, we hypothesized that the dopamine-independent component of *R58E02* valence may depend on one of these other neurotransmitters. We knocked down genes involved in the synthesis or vesicular transport of four other transmitters: *vGlut* for glutamate, *Gad1* for GABA, *vAChT* for acetylcholine, and *Tβh* for octopamine. Of these, knockdown of *vGlut* and *Tβh* in the *R58E02* cells produced effects on valence that were comparable in magnitude to the dopamine reduction: –48% reduction for *Vglut* and –38% for *Tbh* (**Figure 3j**). These results support the idea that *R58E02* valence also requires glutamate and octopamine.

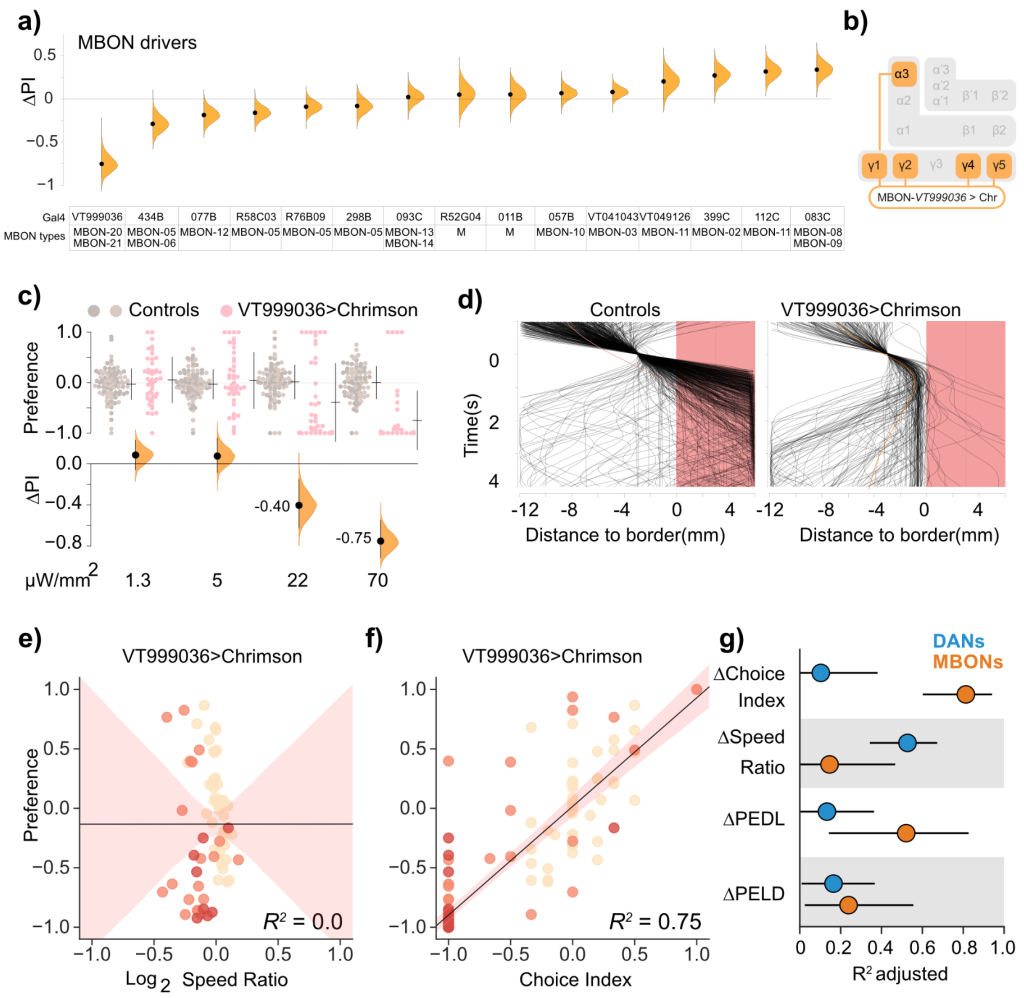

Figure 4. MBONs drive valence via choice effects, not speed effects.

a. A screen of optogenetic Chr valence in 15 MBON-related lines (split-Gal4 and Gal4 drivers). Orange markers show the valence scores (black dots) and distributions (curves) of each cross, comparing test flies with controls. See **Table S1** for effect sizes. The matrix key below shows driver identifiers in the top row, and MBON cell types in which each driver expresses; M denotes multiple cell types. See **Table S2** for further details.

b. A schematic of *VT999036* projections to MBON synaptic-zone subsets. The *VT999036* is reported to drive expression in two MBON types, MBON21 and MBON22 (also known as MBON-γ1γ2 and MBON-γ4γ5) [18].

c. *VT999036>Chr* flies avoided opto-activation at the two highest illumination intensities (22 and 70 μW/mm²). The valence curve is the same data from the screen summary.

d. When *VT999036>Chr* flies move through the choicepoint, they tend to turn away from the light.

e. In *VT999036>Chr* flies, a relationship between preference and speed ratios was absent.

f. In *VT999036>Chr* flies, choice index and preference were related.

g. Summary of regressions of DAN and MBON driver valence. Coefficients of determination for DAN lines (blue dots) and MBON lines (orange dots) are shown for four locomotor metrics as compared to valence (ΔPreference). The four metrics are Δchoice, Δspeed ratio, and the effect sizes of the dark-light and light-dark choice-point exit probabilities (ΔPEDL and ΔPELD, respectively).

DANs and MBONs drive valence with different locomotion patterns

In the mushroom body, the MBONs are known to drive valence [20], and receive synaptic input from the DANs [81]. We asked whether the valence responses mediated by activating DANs and MBONs have similar locomotor features. Screening a panel of MBON drivers for valence (**Figure 4a, S4a-b**), one line, *VT999036*, was found to have the strongest valence. *VT999036* drives expression in MBONs that project to the γ lobe, termed MBON-γ1γ2 and MBON-γ4γ5 cells, also known as MBON types 21 and 22, respectively [18,30] (**Figure 4b, S4e-f, Movie S6, Table S2**). Activation of *VT999036* caused strong aversive valence that (in those flies that crossed from dark to light) was associated with turning away from the light at a light-dark boundary (**Figure 4c-d, Movie S7**). The dark preference of *VT999036>Chr* flies had little relationship to light–dark speed differences but was correlated with a choice index, i.e., fly trajectories at the boundary (**Figure 4e-f**). This contrasts with *R58E02>Chr* and *R15A04>Chr* flies, in which valence is correlated with speed (**Figure 1g-h, S1c-f**).

This observation led us to ask whether the speed/choice dissociation observed in the *R58E02* and *VT999036* lines was part of a trend for DAN and MBON lines generally. We analyzed metrics for all lines in the MBON and DAN screens (**Figure S4a-b, S5a-b**) and used them in regressions of the two screens' valence and speed ratio effect sizes. This analysis indicated that PAM-mediated valences were weakly determined by choice and strongly determined by speed differences (**Figure 4g, S4h-k, S5a-b**). In contrast, MBON-mediated valence was weakly associated with speed and more strongly determined by choice and choice-point exit probabilities (**Figure 4g, S4l-o**). Because lines for both neuronal categories can drive attraction and avoidance, this difference is not easily explained by valence polarity. Still, it suggests that MBON and DAN activities have differential effects on two navigational properties: turning and speed.

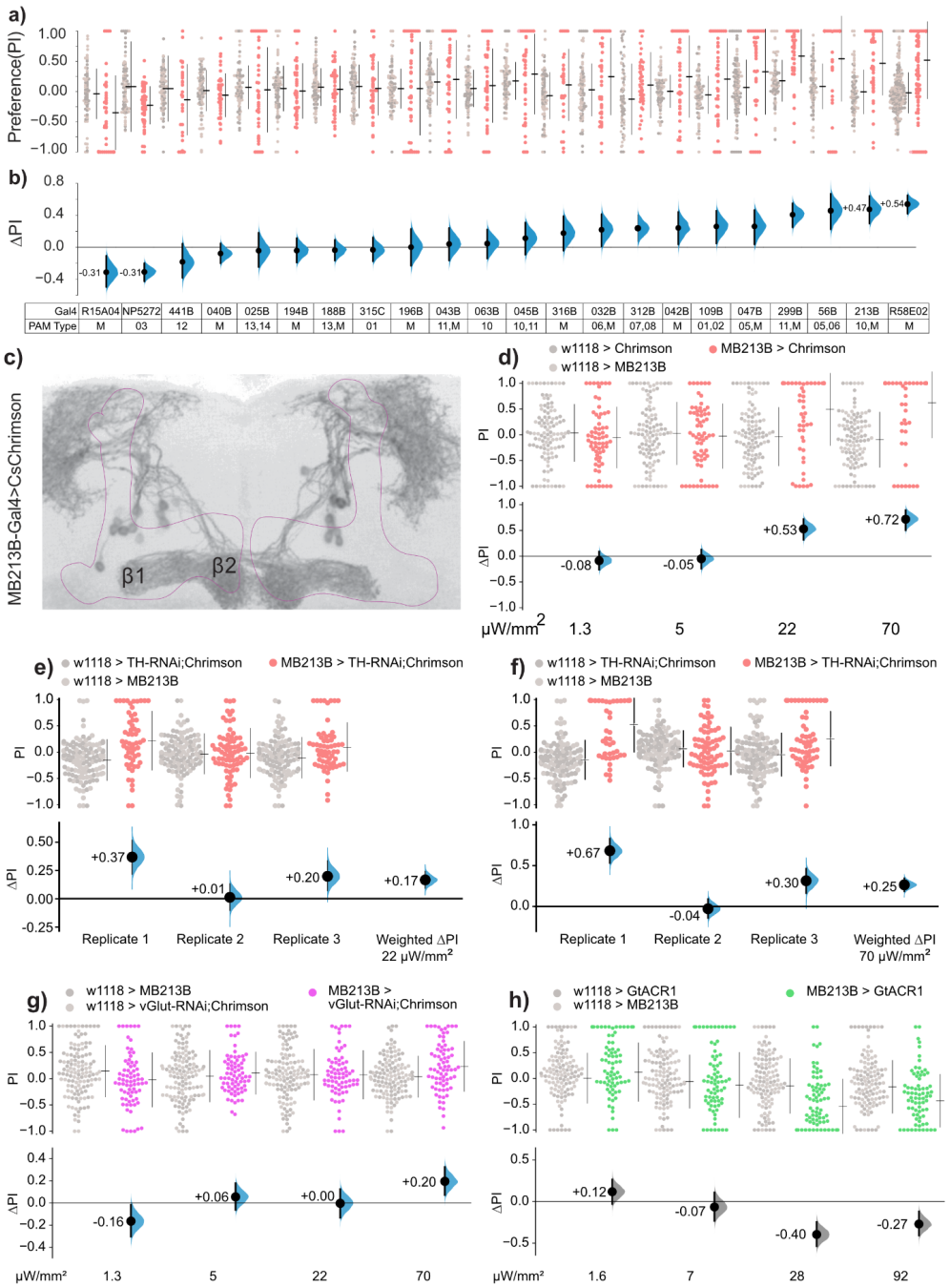

Figure 5. Valence mediated by dopaminergic PAM-β neurons is dependent on both dopamine and glutamate.

a-b. An optogenetic activation screen of 22 PAM-DAN lines identified *MB213B* as the specifically expressing line with the strongest positive valence. Light preference was tested with 72 μW/mm² red light. Table shows the PAM cell types in which each driver expresses; 'M' denotes multiple cell types. See **Table S2** for further details.

c. Expression pattern of *Chr-YFP* with driver *MB213B* showed projections to both zones of the β lobe (zones β1 and β2).

d. Replication of the *MB213B>Chr* screen experiment confirmed that these flies are attracted to optogenetic light at the two highest intensities.
e-f. Meta-analysis of three replicates of *MB213B > TH-RNAi; Chr* yielded weighted ΔPI values of +0.17 at 22 μW/mm^2 and +0.25 at 70 μW/mm^2 (orange curves).
g. Expressing vGlut-RNAi with the *MB213B* driver similarly resulted in reduced (but not ablated) valence.
h. *MB213>ACR1* flies avoided the green-illuminated area.

PAM-β valence is at least partially dependent on dopamine

The opposing valence of *R58E02* and *R15A04* suggested valence heterogeneity in different subsets of PAM DANs. Numerous studies have found that valence-related behaviors like food-seeking, courtship, sleep, and appetitive memory are dependent on different MB sub-compartments and specific DAN subsets [20,22,34,40,49,60,82–85]. To identify PAM types that drive valence, we screened twenty split-Gal4 lines [18,20] and identified several with valence, both negative and positive (**Figure 5a–b**). Of these lines, we focused on *MB213B* as it had the strongest positive valence (**Figure 5b**). This line expresses in the PAM-β1 and PAM-β2 types (PAM4 and PAM10, respectively) with minor expression in the PAM11 (PAM-α1) cells [18] (**Figure 5c, Table S2, Movie S8**). Since valence in *R58E02>Chr* flies is only partially dependent on dopamine, we interrogated *MB213B>Chr* dopamine dependency. Knocking down *TH* in PAM-β cells produced variable results (**Figure S5c-e)**; to resolve these replicate differences, we used inverse-variance meta-analysis using a fixed-effects model to calculate weighted mean-difference estimates at the 22 and 70 μW/mm^2 light intensities [86]. These meta-analyses showed that, when compared to non-RNAi flies (**Figure 5d**), knockdown of *TH* produced a robust though incomplete valence reduction: −68% and −65%, respectively (**Figure 5e-f**). These effects are larger than the *TH-RNAi* knockdown effects for *R58E02>Chr*, which were −42% and −40% for the same light intensities (**Figure 3i**).

PAM-β valence is partially dependent on glutamate

The PAM-β cells have been shown via single-cell RNA-seq to express several other neurotransmitter-related genes, including *vGlut*, *vAChT,* and *Gad1* [34]. As glutamate appears to be a co-transmitter for *R58E02* valence, we examined the effect of *vGlut* knockdown in the specific driver. *MB213B > vGlut-RNAi; Chr* flies displayed valence that was reduced but, like the *TH* knockdown, not eliminated (**Figure 5g**). Thus, it appears that both glutamate and dopamine transmission contribute to valence mediated by the *MB213B* driver, likely through the PAM-β cells.

Pre-existing β-lobe DAN activity contributes to ongoing valence

We asked whether flies are responsive to inhibition of the *MB213B* cells [57]. To drive inhibition, we expressed ACR1 in the *MB213B* cells [74,75]. *MB213B>ACR1* flies displayed negative valence towards green light, indicating that the PAM-β cells are active during this simple behavioral task, and that this activity contributes to valent locomotion (**Figure 5h**).

Discussion

Differences between appetitive learning and acute DAN valence

In this study we provide evidence that a dopaminergic system known to instruct learning also drives acute valence. The PAM DANs instruct appetitive odor learning [9,76], such that subsequent encounters with the same odor will elicit increased approach behavior. Three features distinguish DAN-mediated olfactory learning from DAN-evoked acute valence. First, unlike classical Pavlovian learning—which requires an association between dopamine and a sensory stimulus—acute DAN valence occurs in an experimental environment that is otherwise largely featureless, such that the optogenetic illumination is the only salient sensory stimulus. Thus, the strong elicited valence observed is consistent with non-associative DAN functions that operate independently of external stimuli [22,51]. Second, while the KCs are critical to DAN-mediated sensory associative learning [72,73], activated DAN acute valence has little to no reliance on KCs. Third, while learning has a complete dependency on dopamine receptors in the KCs [25,29,87], *R58E02* PAM valence does not have critical dependencies on either dopamine-receptor function in the KCs or PAM dopamine synthesis. Thus, DAN-dependent learning and DAN valence appear to be distinct processes that act through different circuits and signaling systems.

Differences between DAN and MBON valence

Previously, it was shown that PPL DANs are able to drive optogenetic valence behavior [81]. This study excluded the KCs as the downstream neurons through which the PAM DANs affect valence. This suggests the MBONs as possible mediators, since this class of neurons are major output cells of the MB [18,88–90], and receive synaptic input from the DANs [81].

Under the assumption that DAN valence is mediated by MBONs, we explored some features of valent locomotion as driven by the two cell types. The DAN lines primarily influenced optogenetic light preference by affecting walking speed, while the MBONs, as previously shown [20], had their primary effect by changing trajectories at the light–dark interface, a trend that was independent of valence polarity. There are at least four possible explanations for this difference. First, some of the driver lines (e.g. *VT999036*) capture cells without

MB projections, and these could be contributing to valence, at least in some cases. Second, DANs may have a symmetrical influence on walking, while the MBONs have an asymmetrical effect on walking, perhaps via an algorithm similar to those in Braitenberg vehicles [91]. Third, assuming that DAN valence is mediated by MBON activity, it may be that the MBONs have speed effects when quiescent, but drive turning when highly active, e.g., through distinct downstream circuits with distinct responsiveness to MBON activity. Fourth, the MBON screen may not have included the downstream cells responsible for DAN valence, i.e., other downstream circuits mediate the DAN effects. On this fourth point: the drivers that express in co-zonal DAN and MBON types do not necessarily specify cellular subtypes that share synapses [61,92].

The function of DAN→MBON interactions remains unknown, indeed it is not known whether the DANs drive valent locomotion through the MBONs. Moreover, the idea that DAN valences are exclusively mediated by DAN→MBON synapses in the MB is likely to be incorrect. Connectomic analysis has shown that the PAMs can have pre-synapses in other neuropils [92], suggesting that at least some of the valence effects could be mediated through PAM signaling to non-MB areas. In either case, the speed/turning dissociation is hard to explain with current information.

The appetitive DANs have non-associative functions

These results cast DAN-driven acute valence and olfactory sensory learning as separable processes, wherein the DANs bifurcate to perform two distinct functions. In response to rewarding (or punishing) stimuli, the PAM DANs appear to (1) write olfactory memories to Kandelian-type KC synapses for future reference, and (2) instruct immediate changes in locomotor behavior. Imaging of the MB has shown that DAN activity is closely connected with motor states and locomotion [22,51,93]. Inhibition experiments have revealed that DAN activities guide innate odor avoidance [94], and odor navigation [51]. Similarly, in mammals, reward-related behaviors can be separated into consummatory, motivational, and learning components, of which the latter two are attributable to dopamine function [95]. Organizing parallel signals of a single reward circuit into distinct motivational and associative dopaminergic synapses ensures coherence between valence (the present) and subsequent learned sensory responses (the future). From an evolutionary perspective, we speculate that the motor-function arm predates the associative arm [96], which was inserted when the first sensory systems (taste and olfaction) developed.

A reviewer asked: “Could [the visual associative] pathway be providing a conditioned input to MBONs that is bypassing the inhibited KCs and involve the

PAM DANs?" While green light (such as that used to actuate ACR1) can function as a visual CS+, inhibition of KCs by *MB247-Gal4* abolishes visual learning [38]. In our hands, inhibition using the identical driver leaves valence intact, so the possibility of valence being equivalent to a conditioned visual response appears unlikely. Moreover, while olfactory learning scores and *R58E02* optogenetic valence are of similar magnitudes [97], visual-learning scores are typically <50% of the present valence scores [38,98]. These observations suggest that valence and visual learning are distinct processes.

DAN valence relies on glutamate and octopamine

Knocking down *TH* function reduced *R58E02* valence by roughly half, suggesting the involvement of other neurotransmitters. Screening four other transmitter pathways found that lesions in glutamate transport and octopamine synthesis also produced substantial reductions. At the highest intensity (70 μW/mm^2) the knockdown valence reductions for *TH*, *Vglut*, and *Tbh* were –40%, –48% and –38% respectively; summing these three effect sizes gives –126%. Such an additive 'phenotypic excess' has been observed in a meta-analysis of *Drosophila* olfactory learning [87].

In combination with the narrow driver *MB213B*, knockdowns indicated that dopamine and glutamate were required by the PAM-β cells for normal valence. In previous studies, single-cell RNA sequencing revealed the co-expression of *vGlut*, *Gad1*, *Tbh* and *vAChT* in subpopulations of dopaminergic neurons [34,99]. Together, these findings indicate that the PAM DANs use dopamine, glutamate, and sometimes octopamine as co-transmitters in eliciting optogenetic valence.

Currently, the mechanisms by which dopamine, *Vglut* and *Tbh* act together to mediate valence are unknown. In *Drosophila*, synaptic vesicles at the terminals of DANs undergo hyper-acidification in response to neuronal activity; this is driven by glutamate transport into these vesicles by *Vglut*, which in turn increases the loading of DA [100]. As a result, the effect of *Vglut* knockdown may be due to lower co-release of glutamate and/or reduced loading of DA into synaptic vesicles. DA and glutamate co-transmission is well-documented in mice: in some midbrain neurons, DA and glutamate have been shown to be released from distinct terminals [101–103]. While it is not known if this occurs also in flies, it is possible that DA and glutamate from the PAMs are released from separate termini onto distinct downstream targets. Normal *R58E02* valence also requires *Tbh*. While octopamine is known to be important in both appetitive and aversive memory [104], octopamine co-transmission from the PAMs is novel. How octopamine-dependent, PAM-driven behaviors differ from

DA- and glutamate-dependent behaviors are interesting topics for future studies.

Technical note on interpreting knockdown data

Beyond the *TH-RNAi* immunostaining, we did not assess the molecular effects of the other RNAi manipulations, and it is likely that these RNAi transgenes produced partial knockdowns [77]. Previous work has shown that the *Vglut-RNAi* line used in this paper produces a ~70% mRNA knockdown, whereas the *Gad1-RNAi* line produces an ~82% protein knockdown [49,105]. The remaining lines (*Tbh-RNAi* and *vAChT-RNAi*) were sourced from the Transgenic RNAi Project: the majority of these lines produce knockdowns greater than 50% [106]. Nonetheless, that each of *vGlut-RNAi* and *Tbh-RNAi* produced a substantial reduction in *R58E02* valence demonstrates that the corresponding neurotransmitters play a role in *R58E02* valence. In *vAChT-RNAi* and *Gad1-RNAi*, neither of which produced appreciable changes to *R58E02* valence, we cannot discern whether this was due to poor RNAi efficiency or that those transmitters play no role. Thus, the effect sizes from the RNAi experiments should correctly be interpreted as lower bounds on the potential impact of each gene's loss of function. Even though the individual knockdown effect sizes are likely underestimated, nevertheless, in at least one experiment the sum of the *TH*, *Vglut*, and *Tbh* knockdown effect sizes exceeds 100% (**Figure 3J**). Investigating this effect-size surfeit is a possible direction of future experimentation.

Possible explanations for valence variability

Of this study's many limitations, of note is the sometimes pronounced variability in results between experimental iterations. For example, *R58E02 > Chr* flies showed variable valence when tested by different experimenters at different times (**Figure 1e, 3g**). Similarly, *MB213B > Chr; TH-RNAi* flies showed variable valence (**Figure S5c-e**). One likely contributor is sampling error, a routine issue in behavioral data [107]. For several dopamine-depletion experiments, we mitigated sampling error using meta-analysis to calculate a more precise effect size [107]. A second possibility is that neurotransmitter dependencies may vary between iterations due to uncontrolled changes during development or internal state. For example, the loss of dopamine may sometimes lead to developmental compensation, such as neurotransmitter switching or circuit adjustments. In mammals, neurotransmitter switching in dopaminergic cells can occur as a result of stimuli such as odor or light stress [108–110]. In *Drosophila*, the expression of *vGlut* in DANs increases as dopamine is depleted either pharmacologically or due to aging [111]. It is possible that, as RNAi depletes TH, the PAM-β cells switch to glutamate as a substitute transmitter (but see the notes on effect-size surfeit above). A third possible

explanation of the variability is that, due to one or more uncontrolled variables, some neurons' valence is susceptible to internal state. Imaging has shown that PAM-γ cells display activities that vary depending on state, such as starvation and walking [22,57]. If, for example, PAM-β baseline activity is high, it might be expected that the valence due to further activation will be small. Conversely, in a low baseline activity state, stimulation of these cells would be expected to result in a large effect. Recent studies have described high variability between different optogenetic valence assays [62,65], suggesting that optogenetic valence is not generalizable between different behavioral tasks. Since different sensory modalities and/or associative circuits may be employed for different tasks, this is not unexpected. Like all cognitive constructs, so-called "valence" could benefit from systematic investigations by multiple groups across behavioral paradigms.

Are dopamine-related driver valences dependent on DANs?

A reviewer asked about the possible role of cells outside the PAM DANs being responsible for some part of the valence. "Could [optic lobe] ectopic expression also explain why knockdown of DA production in [*R58E02*] had an incomplete effect?" While this could explain the residual valence, we consider it to be unlikely. First, the cells in the optic lobe have been reported to be glia: "[*R58E02*] strongly labels the PAM cluster neurons and glial cells in the optic lobes with little expression elsewhere" [76]. Second, our screen of the PAM-DAN split-Gal4s shows that a number of them give positive valence, generalizing the phenomenon beyond the *R58E02* driver. Third, the *MB213B* split-Gal4 driver (which does not have any detectable expression outside of the PAM DANs) has a positive valence that—like *R58E02*—is only partially reduced by dopamine knockdown. These observations support the idea that the valence observed in knockdown animals is attributable to PAM-DAN activity.

Important questions beyond the study's scope

Reviewers also asked: "How can optogenetic activation of DANs and their postsynaptic MBONs drive distinct locomotor behaviors? What role does co-transmission of different neurotransmitters play in this behavioral modulation? Why do some DANs drive attraction but a subset of this larger population drive aversion?" and "If the olfactory stimulus is removed from the equation…what is the neurophysiological signal that dopamine acts on to modulate walking speed?" These are all interesting, relevant questions that go beyond the present study's scope and could be addressed in future studies.

Ongoing DAN activities shape behavior

That flies avoid silencing the PAM-β dopaminergic cells indicates that stimulus-independent DAN activities influence behavior. In the context of Pavlovian conditioning, dopamine has been closely associated with its role as a transient, stimulus-evoked signal, while this result indicates that some of the PAM neurons are active even in a chamber lacking food, odor, shock, or other stimuli. Physiological recordings show that, along with sucrose responses, PAM-γ activities are correlated with motion and guide odor-tracking behavior, supporting the idea that PAM-DAN activities both respond to and steer locomotor behavior [22,51]. In our optogenetic preference screen, activity in various PAM DAN populations were rewarding, aversive or showed little preference effect, indicating that there is a diversity of functions between different DAN types, consistent with findings for learning and memory [9,11,14,26–34,76]. The bidirectionality of the attractive and aversive effects of increasing and decreasing activity in this dopaminergic system is similar to valence responses to activation and inhibition of dopaminergic cells in the mammalian ventral tegmental area [8,112,113] and is reminiscent of the increases and decreases in activity in that area that occur during positive and negative reward prediction errors, respectively [114]. Whole-brain imaging in the nematode has shown that global brain dynamics track closely with locomotion [115], suggesting that the primary overarching function of brains is to coordinate motor function. That the mushroom-body DANs drive preference-related locomotion suggest that they have two types of valence roles: informing responses to future experiences while steering current behavior.

Methods

Fly strains

Flies were cultured on a standard fly medium [116] at 25°C and 60% humidity in a 12 h light: 12 h dark cycle. Wild-type flies were a cantonized w^{1118} line. The DAN and MBON split-Gal4 lines described in [18] were a gift from Gerry Rubin (Howard Hughes Medical Institute), except for VT041043-Gal4 [105] and VT49126-Gal4 [30], which were obtained from the Vienna Drosophila Resource Center (VDRC). *VT999036* was a gift from Barry Dickson (Howard Hughes Medical Institute). The Gal4 transgenic lines were obtained from the Bloomington Drosophila Stock Center (BDSC) and included: *R58E02-Gal4* [10], *R15A04-Gal4* [69], *20x-UAS-CsChrimson [66]*, 13X-LexAOp2-GtACR1 [117], *MB247-Gal4 [118]*, *MB247-LexA* [119]. *R53C03-Gal4* [18], *R76B09-Gal4* [30], *R52G04-Gal4* [20]. *NP5272-Gal4* [16] were obtained from the Kyoto Stock Center (DGRC). The RNAi lines used were: Dop1R1 (KK 107058), Dop1R2 (KK 105324), Dop2R (GD 11471), vGlut (KK104324), and TH (KK 108879), obtained from VDRC; as well as Gad1 (BDSC_51794), Tβh (BDSC_76062), and vAChT (BDSC_80435) from the Transgenic RNAi Project [106]. Supplemental Table 1 provides detailed descriptions of genotypes shown in each figure

Transgenic animal preparation

Gal4, *UAS-CsChrimson*, and *UAS-ACR1* crosses were maintained at 25°C and 60% humidity, in darkness. Groups of 25 newly eclosed flies were separated into vials for 2–3 days (in the dark at 25°C) before behavioral phenotyping. Control flies were generated by crossing the driver or responder line with a wild-type w^{1118} strain (originally bought from VDRC), and raising the progeny under identical regimes to those used for the test flies. A stock solution of all-*trans*-retinal was prepared in 95% ethanol (w/v) and mixed with warm, liquefied fly food. Each vial was covered with aluminum foil and incubated at 25°C in the dark. Before optogenetic experiments, 3–5 day-old male flies were fed 0.5 mM all-*trans*-retinal (Sigma) for 2–3 days at 25°C in the dark.

Drug treatment

Male flies (3–5 days old) were placed on 1% agar containing 5% sucrose, 10 mg/mL 3-iodo-L-tyrosine (3-IY, Sigma), and 0.5 mM all-trans-retinal for 2–3 days at 25°C in the dark prior to behavioral testing. Control flies were fed on the same food but with 3-IY omitted.

Immunohistochemistry

Immunohistochemistry was performed as previously described [75]. Briefly, brains were dissected in phosphate buffered saline (PBS) and fixed in PBS with 4% paraformaldehyde (Electron Microscopy Sciences) for 20 min. Samples were

washed three times with PBT (PBS + 1% Triton X-100) and blocked with 5% normal goat serum for 1 h. Samples were then incubated with primary antibodies overnight at 4°C. After three additional washes with PBT, samples were incubated with secondary antibodies overnight at 4°C. The following primary and secondary antibodies were used: mouse α-DLG1 (4F3 α-DISCS LARGE 1, Developmental Studies Hybridoma Bank, 1:200 dilution), Alexa Fluor 488 rabbit α-GFP-IgG (A-21311, Molecular Probes, 1:200 dilution), Alexa-Fluor 568 goat anti-mouse (1:200, Molecular Probes).

Confocal laser microscopy and neuroanatomy

Confocal images were acquired under a Zeiss LSM 710 microscope at a z-step of 0.5 µm using 20×, 40×, or 63× objectives. Images were analyzed using ImageJ software. Images are shown in black and white as a maximum projection intensity (MIP) of the green channel. The stacks were visualized and analyzed with the FIJI distribution (www.fiji.sc) of ImageJ (NIH). Outlines of α-Dlg1 expression in the mushroom body were traced with Adobe Illustrator. Projection patterns and zonal identity were assigned as previously described [18]. When not verified by microscopy, cell types and projection patterns were classified by review of published reports (Table S2) [18,30,31,60,76,105].

Optogenetic response assay

Behavior experiments were performed as previously described [75]. Each behavioral arena was cut with 55 × 4 mm stadium/discorectangle geometry; 15 such arenas were cut from 1.5 mm-thick transparent acrylic. During the behavioral assay, arenas were covered with a transparent acrylic lid. As previously described [3], flies were anesthetized on ice before loading into each chamber in the dark. The arena multiplex was kept under infrared (IR) light at 25°C for 2–3 min before starting the assay. Flies were aroused by shaking the arenas just before starting the experiment. All behaviors were recorded under IR light. The multiplex was illuminated with red or green light from a mini-projector positioned above the arena (Optoma ML750). For *CsChrimson* experiments, flies were illuminated with four red-light intensities: 1.3, 5, 22, and 70 µW/mm^2. For *ACR1* experiments, the flies were illuminated with four green light intensities: 1.6, 7, 28, and 92 µW/mm^2. The colored light intensity was varied by changing the level of the respective RGB component of the projected color. For each experiment, the arenas were illuminated for 60 s with equal-sized quadrants to produce a banded light-dark-light-dark pattern.

Video tracking

The behavior arena was imaged with a monochrome camera (Guppy-046 B, Allied Vision) with two IR longpass filters in series (IR Filter IR850, Green.L).

Videos were processed in real time with CRITTA software written in LabView [75]. The x-y coordinates of each fly's head were individually tracked (at 25 frames per second) using CRITTA's tracking feature. CRITTA was also used to control the timing, hue and intensity of the illumination, and to count the number of flies in each quadrant for each video frame. The light borders were identified and calibrated using a function of the CRITTA plugin, which illuminates quadrants at low intensity and captures an image of the arenas (with camera IR filters removed). The plugin software calculates the horizontal intensity profile of each arena and finds the center of each light-dark boundary using an edge-detection algorithm. The light-border drift between presented experiments was 330 µm (95CI 230 µm; 430 µm). Between the light and dark regions, there is a light gradient that was a mean 670 µm wide with a range of 420 to 1040 µm. This was measured from 45 images of boundaries from 15 chambers, and scored as all the pixels falling between high (light-on) and low-intensity light regions.

Olfactory conditioning

Conditioning was performed as previously described [75,120]. Briefly, each behavior chamber was 50 mm long, 5 mm wide, and 1.3 mm high; the floor and ceiling of each chamber were composed of transparent shock boards made from indium tin oxide electrodes printed on glass (Visiontek UK). Odorized air was pumped into each end of each arena at 500 mL/min. The odors were 4-methylcyclohexanol (MCH) at 9 parts per million (ppm) and 3-octanol (OCT) at 6 ppm, as measured with a photoionization detector (RAE systems, ppbRAE3000). The air exited the chamber via two vents located in the middle, creating two odor partitions in the conditioning area. Each experiment was performed with 4–6 flies. For opto-conditioning, flies were presented with either OCT or MCH odor paired with green light (515 nm, 28 $\mu W/mm^2$), followed by another odor without visible light (IR light only). During shock-conditioning, the presentation of either OCT or MCH was coupled with 12 electric shocks of 1 s duration at 60V [14]. Conditioned-odor preference (memory) was tested by the presentation of both odors, one from each side. For each of the two odors, a half performance index (PI) was calculated according to the fly position coordinates during the last 30 s of each testing phase; for each iteration, data from odor pairs were averaged to obtain a full PI [121].

Preference and speed analysis

Custom Python scripts were used for data processing, analysis and visualization. The scripts integrated several routines from NumPy, pandas, matplotlib, and seaborn. For every fly, the x-y coordinates of the head location (recorded at 25 frames per second) underwent rolling-window smoothing,

using a centered 1 s-wide triangular window. The following metrics were obtained (for every fly) for the last 30 s of each test session:

$$Preference\ Index\ (PI)\ = \frac{time\ in\ light - time\ in\ dark}{total\ time}$$

$$log_2\ Speed\ Ratio\ (LSR)\ =\ log_2\left(\frac{mean\ speed\ in\ light}{mean\ speed\ in\ dark}\right)$$

While all flies could be assigned a PI, the $\log_2$ Speed Ratio (LSR) could be computed only for flies that moved in both light and dark regions during the illumination epoch. Flies that remained stationary for the entire illumination epoch, or remained in only the light or dark zones, were excluded from the speed ratio calculation. Flies that start and remain in either the dark or light zone throughout an epoch, but still move within the zone, are assigned an extreme PI (–1.0 or +1.0, respectively).

Choice-zone trajectory analysis

A choice trajectory was defined as any transit in and out of a choice-zone defined to extend 3 mm in either direction from all three light borders. Trajectories were identified for every fly that approached the choice zone, and the following metrics were computed:

$$Choice\ Index\ (CI)\ =\ \frac{trajectories\ exiting\ to\ light - trajectories\ exiting\ to\ dark}{total\ trajectories}$$

$$Proportion\ of\ Exits\ from\ Dark\ to\ Light\ (PEDL)\ = \frac{entries\ from\ the\ dark\ exiting\ to\ light}{total\ entries\ from\ the\ dark}$$

$$Proportion\ of\ Exits\ from\ Light\ to\ Dark\ (PELD)\ = \frac{entries\ from\ the\ light\ exiting\ to\ dark}{total\ entries\ from\ the\ light}$$

The above three metrics were computed for all flies that entered a choice zone at least once during the illumination epoch. Flies that did not make such a crossing during the epoch (i.e. remained on one side for the epoch duration) were necessarily excluded from boundary trajectory analysis. Note that as flies can enter a choice zone without ever subsequently crossing from dark to light (or vice versa), not all flies with a choice index could also be assigned a speed ratio; this would include flies that consistently made choice-zone reversals without crossing a light-dark boundary. Thus, the choice-zone analysis necessarily excludes flies that never cross a light-dark boundary.

Effect-size regression

To compare the valence effect size (Δ Preference) with locomotion effect sizes, we calculated Δ values for four locomotion metrics.

$$\Delta\ Speed\ Ratio\ (\Delta LSR)\ =\ mean\ LSR_{test} - mean\ LSR_{control}$$

$$\Delta\ Choice\ Index\ (\Delta CI)\ =\ mean\ CI_{test} - mean\ CI_{control}$$

$$\Delta\ PELD\ =\ mean\ PELD_{test} -\ mean\ PELD_{control}$$

$$\Delta\ PEDL\ =\ mean\ PEDL_{test} -\ mean\ PEDL_{control}$$

Each Δ value was calculated for the two highest illumination intensity epochs (22 and 70 μW/mm2) for all PAM or MBON lines. As the locomotion metrics require that a fly crosses the light–dark boundary at least once, some flies were necessarily censored from this analysis.

Each set of effect sizes was subjected to regression against the corresponding Δ Preference values. Regression was performed with the linear least-squares method of the SciPy library. For both mean differences and coefficients of determination (R^2), distributions and 95% confidence intervals were obtained from 3,000 resamples, using bias correction and acceleration [122] with the scikits.bootstrap package.

Meta-analysis of dopamine-depleting interventions

Different dopamine loss-of-function experiments with *R58E02>Chr* were done using 3-iodo-tyrosine, *TH-RNAi*, or *TH-RNAi* with *Dicer2* at several light intensities, a total of 15 valence experiments. We aimed to estimate the effect of reducing dopamine function in the *R58E02* cells as a percentage of wild-type behavior [87,97]. Using data from three replicates of the *R58E02>Chr* experiment, we first calculated a mean ΔPI (controls) valence via simple averaging for the 5, 22 and 70 μW/mm^2 light conditions. The ΔPIs for each dopamine-depleting intervention were then expressed as a percentage of the control value [97] for each of three light intensities .

$$Mean\ \Delta PI\ of\ controls\ =\ \frac{\Sigma\ \Delta PI\ across\ 3\ replicates}{3}$$

$$Percent\ of\ control\ (\%\Delta PI)\ =\ \frac{Intervention\ \Delta PI}{Mean\ control\ \Delta PI} \times 100$$

The data used for calculating the mean ΔPI (controls) value is presented in **Figures 3g**, **S3d** and **S3e**. The data used for calculating % of control for each intervention is presented in figures: **S3b** (3-iodo-tyrosine); **3h**, **S3f** and **S3g** (*TH-RNAi*); **S3c** (*TH-RNAi* with *Dicer2*).

Meta-analysis of experimental replicates

For replicates of the *MB213> TH-RNAi; Chrimson* experiment, we performed inverse-variance meta-analysis with a fixed-effects model. A weighted effect size was calculated as follows:

$$\theta_{weighted} = \frac{\Sigma(\hat{\theta}_i w_i)}{\Sigma w_i}$$

Where:

$$\hat{\theta}_i = Effect\ size\ (mean\ difference)\ for\ replicate\ i$$

$$w_i = Weight\ for\ replicate\ i = \frac{1}{s_i^2}$$

$$s_i^2 = Pooled\ control + test\ variance\ for\ replicate\ i$$

Statistics

Effect sizes were used for data analysis and interpretation. Summary measures for each group were plotted as a vertical gapped line: the ends of the line correspond to the ±standard deviations of the group, and the mean itself plotted as a gap. Effect sizes were reported for each driver line as mean differences between controls and test animals for all the behavioral metrics [123]. Two controls (driver and responder) were grouped together and the averaged mean of the two controls was used to calculate the mean difference between control and test flies. In text form, the mean differences and their 95% confidence intervals are presented as "mean [95CI lower bound, upper bound]." The mean differences are depicted as black dots, with the 95% confidence interval indicated by error bars. Where possible, each error bar is accompanied with a filled curve displaying the distribution of mean differences, as calculated by bootstrap resampling. Bootstrapped distributions are robust for non-normal data [124].

P values were calculated by the Mann-Whitney rank method in SciPy and presented *pro forma* only: following best practice, no significance tests were conducted [123]. The behavioral sample sizes (typically N = 45, 45, 45) had a power of >0.8, assuming $\alpha = 0.05$ and an effect size of Hedges' g = 0.6 SD. All error bars for mean differences represent the 95% confidence intervals.

Genotypes and statistics for control and test flies for each panel are provided in the Supplementary Table (**Table S1**), as are details of the mega-analysis of mutant effect sizes (**Figure 4g**) incorporating data from across the study.

Data availability

All data generated for this paper are available for download from Zenodo (https://doi.org/10.5281/zenodo.7747425).

Code availability

All code used for analysis of data is available for download from Zenodo (https://doi.org/10.5281/zenodo.7747425).

Acknowledgments

We thank Gerald Rubin (Howard Hughes Medical Institute) for the DAN and MBON split-Gal4 lines, Barry Dickson (Howard Hughes Medical Institute) for providing the *VT999036* flies. We thank Dr. Jessica Edwards of Insight Editing London for critical review of the manuscript before submission.

Author Contributions

Conceptualization: FM and ACC; Experiment design: FM, YM and ACC; Methodology: FM, JCS and ACC; Software: JH (Python), and JCS (CRITTA, LabView); Data Analysis: JH (Python), FM (Python), YM (Python) and JCS (LabView); Investigation: FM and YM (genetics, fly husbandry, behavior, immunohistochemistry, and microscopy), XYZ (behavior, brain dissection, immunohistochemistry, microscopy), SO (memory); Resources: JCS (instrumentation); Writing – Original Draft: FM; Writing – Revision: FM, YM, and ACC; Visualization: FM, YM, JH, ACC; Supervision: ACC; Project Administration: ACC; Funding Acquisition: ACC.

Competing interests

The authors declare no competing interests.

Funding

FM, YM, SO, XYZ, and ACC were supported by grants MOE-2013-T2-2-054, MOE2017-T2-1-089, and MOE2019-T2-1-133 from the Ministry of Education, Singapore; JCS and ACC were supported by grants 1231AFG030 and 1431AFG120 from the A*STAR Joint Council Office. YM was supported by Duke-NUS Medical School and by a President's Graduate Fellowship funded through the Jasmine Scholarship; JH was supported by the A*STAR Scientific Scholars Fund; SO was supported by a Khoo Postdoctoral Fellowship Award and an NMRC Young Investigator Research Grant; XYZ was supported by a Yong Loo Lin School of Medicine scholarship. The authors were supported by a Biomedical Research Council block grant to the Institute of Molecular and Cell Biology, and a Duke-NUS Medical School grant to ACC.

References

1. Anderson DJ, Adolphs R. A framework for studying emotions across species. Cell. 2014;157: 187–200.

2. Darwin C. The Expression of the Emotions in Man and Animals. Project Gutenberg; 1899.

3. Mohammad F, Aryal S, Ho J, Stewart JC, Norman NA, Tan TL, et al. Ancient Anxiety Pathways Influence Drosophila Defense Behaviors. Curr Biol. 2016;26: 981–986.

4. Bargmann CI. Beyond the connectome: how neuromodulators shape neural circuits. Bioessays. 2012;34: 458–465.

5. Marder E. Neuromodulation of neuronal circuits: back to the future. Neuron. 2012;76: 1–11.

6. Schultz W. Multiple dopamine functions at different time courses. Annu Rev Neurosci. 2007;30: 259–288.

7. Bromberg-Martin ES, Matsumoto M, Hikosaka O. Dopamine in motivational control: rewarding, aversive, and alerting. Neuron. 2010;68: 815–834.

8. Namburi P, Al-Hasani R, Calhoon GG, Bruchas MR, Tye KM. Architectural Representation of Valence in the Limbic System. Neuropsychopharmacology. 2016;41: 1697–1715.

9. Burke CJ, Huetteroth W, Owald D, Perisse E, Krashes MJ, Das G, et al. Layered reward signalling through octopamine and dopamine in Drosophila. Nature. 2012;492: 433–437.

10. Liu C, Plaçais P-Y, Yamagata N, Pfeiffer BD, Aso Y, Friedrich AB, et al. A subset of dopamine neurons signals reward for odour memory in Drosophila. Nature. 2012;488: 512–516.

11. Lin S, Owald D, Chandra V, Talbot C, Huetteroth W, Waddell S. Neural correlates of water reward in thirsty Drosophila. Nat Neurosci. 2014;17: 1536–1542.

12. Han KA, Millar NS, Grotewiel MS, Davis RL. DAMB, a novel dopamine receptor expressed specifically in Drosophila mushroom bodies. Neuron. 1996;16: 1127–1135.

13. Kim Y-C, Lee H-G, Han K-A. D1 dopamine receptor dDA1 is required in the mushroom body neurons for aversive and appetitive learning in Drosophila. J Neurosci. 2007;27: 7640–7647.

14. Claridge-Chang A, Roorda RD, Vrontou E, Sjulson L, Li H, Hirsh J, et al. Writing memories with light-addressable reinforcement circuitry. Cell. 2009;139: 405–415.

15. Schroll C, Riemensperger T, Bucher D, Ehmer J, Völler T, Erbguth K, et al. Light-Induced Activation of Distinct Modulatory Neurons Triggers

Appetitive or Aversive Learning in Drosophila Larvae. Curr Biol. 2006;16: 1741–1747.

16. Aso Y, Herb A, Ogueta M, Siwanowicz I, Templier T, Friedrich AB, et al. Three dopamine pathways induce aversive odor memories with different stability. PLoS Genet. 2012;8: e1002768.

17. Busto GU, Cervantes-Sandoval I, Davis RL. Olfactory learning in Drosophila. Physiology . 2010;25: 338–346.

18. Aso Y, Hattori D, Yu Y, Johnston RM, Iyer NA, Ngo T-TB, et al. The neuronal architecture of the mushroom body provides a logic for associative learning. Elife. 2014;3: e04577.

19. Takemura S-Y, Aso Y, Hige T, Wong A, Lu Z, Shan Xu C, et al. A connectome of a learning and memory center in the adult Drosophila brain. Elife. 2017;6. doi:10.7554/elife.26975

20. Aso Y, Sitaraman D, Ichinose T, Kaun KR, Vogt K, Belliart-Guérin G, et al. Mushroom body output neurons encode valence and guide memory-based action selection in Drosophila. Elife. 2014;3: e04580.

21. Hige T, Aso Y, Modi MN, Rubin GM, Turner GC. Heterosynaptic Plasticity Underlies Aversive Olfactory Learning in Drosophila. Neuron. 2015;88: 985–998.

22. Cohn R, Morantte I, Ruta V. Coordinated and Compartmentalized Neuromodulation Shapes Sensory Processing in Drosophila. Cell. 2015;163: 1742–1755.

23. Owald D, Waddell S. Olfactory learning skews mushroom body output pathways to steer behavioral choice in Drosophila. Curr Opin Neurobiol. 2015;35: 178–184.

24. Schwaerzel M, Monastirioti M, Scholz H, Friggi-Grelin F, Birman S, Heisenberg M. Dopamine and octopamine differentiate between aversive and appetitive olfactory memories in Drosophila. J Neurosci. 2003;23: 10495–10502.

25. Kim Y-C, Lee H-G, Han K-A. D1 dopamine receptor dDA1 is required in the mushroom body neurons for aversive and appetitive learning in Drosophila. J Neurosci. 2007;27: 7640–7647.

26. Krashes MJ, DasGupta S, Vreede A, White B, Armstrong JD, Waddell S. A neural circuit mechanism integrating motivational state with memory expression in Drosophila. Cell. 2009;139: 416–427.

27. Aso Y, Siwanowicz I, Bräcker L, Ito K, Kitamoto T, Tanimoto H. Specific dopaminergic neurons for the formation of labile aversive memory. Curr Biol. 2010;20: 1445–1451.

28. Aso Y, Herb A, Ogueta M, Siwanowicz I, Templier T, Friedrich AB, et al. Three Dopamine Pathways Induce Aversive Odor Memories with Different

Stability. Rulifson E, editor. 2012. doi:10.1371/journal.pgen.1002768

29. Qin H, Cressy M, Li W, Coravos JS, Izzi SA, Dubnau J. Gamma neurons mediate dopaminergic input during aversive olfactory memory formation in Drosophila. Curr Biol. 2012;22: 608–614.

30. Shuai Y, Hirokawa A, Ai Y, Zhang M, Li W, Zhong Y. Dissecting neural pathways for forgetting in Drosophila olfactory aversive memory. Proc Natl Acad Sci U S A. 2015;112: E6663–72.

31. Yamagata N, Ichinose T, Aso Y, Plaçais P-Y, Friedrich AB, Sima RJ, et al. Distinct dopamine neurons mediate reward signals for short- and long-term memories. Proc Natl Acad Sci U S A. 2015;112: 578–583.

32. Aso Y, Rubin GM. Dopaminergic neurons write and update memories with cell-type-specific rules. Elife. 2016;5. doi:10.7554/eLife.16135

33. Berry JA, Phan A, Davis RL. Dopamine Neurons Mediate Learning and Forgetting through Bidirectional Modulation of a Memory Trace. Cell Rep. 2018;25: 651–662.e5.

34. Aso Y, Ray RP, Long X, Bushey D, Cichewicz K, Ngo T-T, et al. Nitric oxide acts as a cotransmitter in a subset of dopaminergic neurons to diversify memory dynamics. Elife. 2019;8. doi:10.7554/eLife.49257

35. Siju KP, Bräcker LB, Grunwald Kadow IC. Neural mechanisms of context-dependent processing of CO2 avoidance behavior in fruit flies. Fly . 2014;8: 68–74.

36. Dolan M-J, Belliart-Guérin G, Bates AS, Frechter S, Lampin-Saint-Amaux A, Aso Y, et al. Communication from Learned to Innate Olfactory Processing Centers Is Required for Memory Retrieval in Drosophila. Neuron. 2018;100: 651–668.e8.

37. Dolan M-J, Frechter S, Bates AS, Dan C, Huoviala P, Roberts RJ, et al. Neurogenetic dissection of the Drosophila lateral horn reveals major outputs, diverse behavioural functions, and interactions with the mushroom body. Elife. 2019;8. doi:10.7554/eLife.43079

38. Vogt K, Schnaitmann C, Dylla KV, Knapek S, Aso Y, Rubin GM, et al. Shared mushroom body circuits underlie visual and olfactory memories in Drosophila | eLife. Elife. 2014;3: e02395.

39. Ueno T, Tomita J, Tanimoto H, Endo K, Ito K, Kume S, et al. Identification of a dopamine pathway that regulates sleep and arousal in Drosophila. Nat Neurosci. 2012;15: 1516–1523.

40. Sitaraman D, Aso Y, Rubin GM, Nitabach MN. Control of Sleep by Dopaminergic Inputs to the Drosophila Mushroom Body. Front Neural Circuits. 2015;9: 73.

41. Bang S, Hyun S, Hong S-T, Kang J, Jeong K, Park J-J, et al. Dopamine signalling in mushroom bodies regulates temperature-preference

behaviour in Drosophila. PLoS Genet. 2011;7: e1001346.

42. Azanchi R, Kaun KR, Heberlein U. Competing dopamine neurons drive oviposition choice for ethanol in Drosophila. Proc Natl Acad Sci U S A. 2013;110: 21153–21158.

43. Lim J, Fernandez AI, Hinojos SJ, Aranda GP, James J, Seong C-S, et al. The mushroom body D1 dopamine receptor controls innate courtship drive. Genes Brain Behav. 2018;17: 158–167.

44. Aimon S, Katsuki T, Jia T, Grosenick L, Broxton M, Deisseroth K, et al. Fast near-whole-brain imaging in adult Drosophila during responses to stimuli and behavior. PLoS Biol. 2019;17: e2006732.

45. Liu L, Wolf R, Ernst R, Heisenberg M. Context generalization in Drosophila visual learning requires the mushroom bodies. Nature. 1999;400: 753–756.

46. Zhang K, Guo JZ, Peng Y, Xi W, Guo A. Dopamine-mushroom body circuit regulates saliency-based decision-making in Drosophila. Science. 2007;316: 1901–1904.

47. van Swinderen B, McCartney A, Kauffman S, Flores K, Agrawal K, Wagner J, et al. Shared visual attention and memory systems in the Drosophila brain. PLoS One. 2009;4: e5989.

48. Manjila SB, Kuruvilla M, Ferveur J-F, Sane SP, Hasan G. Extended Flight Bouts Require Disinhibition from GABAergic Mushroom Body Neurons. Curr Biol. 2019;29: 283–293.e5.

49. Tsao C-H, Chen C-C, Lin C-H, Yang H-Y, Lin S. Drosophila mushroom bodies integrate hunger and satiety signals to control innate food-seeking behavior. Elife. 2018;7. doi:10.7554/eLife.35264

50. Sayin S, De Backer J-F, Siju KP, Wosniack ME, Lewis LP, Frisch L-M, et al. A Neural Circuit Arbitrates between Persistence and Withdrawal in Hungry Drosophila. Neuron. 2019;104: 544–558.e6.

51. Zolin A, Cohn R, Pang R, Siliciano AF, Fairhall AL, Ruta V. Context-dependent representations of movement in Drosophila dopaminergic reinforcement pathways. Nat Neurosci. 2021;24: 1555–1566.

52. Hattori D, Aso Y, Swartz KJ, Rubin GM, Abbott LF, Axel R. Representations of Novelty and Familiarity in a Mushroom Body Compartment. Cell. 2017;169: 956–969.e17.

53. Colomb J, Kaiser L, Chabaud M-A, Preat T. Parametric and genetic analysis of Drosophila appetitive long-term memory and sugar motivation. Genes Brain Behav. 2009;8: 407–415.

54. Landayan D, Feldman DS, Wolf FW. Satiation state-dependent dopaminergic control of foraging in Drosophila. Sci Rep. 2018;8: 5777.

55. Grunwald Kadow IC. State-dependent plasticity of innate behavior in fruit flies. Curr Opin Neurobiol. 2019;54: 60–65.

56. Jacob PF, Vargas-Gutierrez P, Okray Z, Vietti-Michelina S, Felsenberg J, Waddell S. Prior experience conditionally inhibits the expression of new learning in Drosophila. Curr Biol. 2021;31: 3490–3503.e3.

57. Siju KP, Štih V, Aimon S, Gjorgjieva J, Portugues R, Grunwald Kadow IC. Valence and State-Dependent Population Coding in Dopaminergic Neurons in the Fly Mushroom Body. Curr Biol. 2020;30: 2104–2115.e4.

58. Jovanoski KD, Duquenoy L, Mitchell J, Kapoor I, Treiber CD, Croset V, et al. Dopaminergic systems create reward seeking despite adverse consequences. Nature. 2023. doi:10.1038/s41586-023-06671-8

59. Cheng KY, Colbath RA, Frye MA. Olfactory and Neuromodulatory Signals Reverse Visual Object Avoidance to Approach in Drosophila. Curr Biol. 2019;29: 2058–2065.e2.

60. Huetteroth W, Perisse E, Lin S, Klappenbach M, Burke C, Waddell S. Sweet taste and nutrient value subdivide rewarding dopaminergic neurons in Drosophila. Curr Biol. 2015;25: 751–758.

61. Otto N, Pleijzier MW, Morgan IC, Edmondson-Stait AJ, Heinz KJ, Stark I, et al. Input Connectivity Reveals Additional Heterogeneity of Dopaminergic Reinforcement in Drosophila. Curr Biol. 2020;30: 3200–3211.e8.

62. Stern U, Srivastava H, Chen H-L, Mohammad F, Claridge-Chang A, Yang C-H. Learning a Spatial Task by Trial and Error in Drosophila. Curr Biol. 2019;29: 2517–2525.e5.

63. Mishra A, Cronley P, Ganesan M, Schulz DJ, Zars T. Dopaminergic neurons can influence heat-box place learning in Drosophila. J Neurogenet. 2020;34: 115–122.

64. Lesar A, Tahir J, Wolk J, Gershow M. Switch-like and persistent memory formation in individual Drosophila larvae. Elife. 2021;10. doi:10.7554/eLife.70317

65. Rohrsen C, Kumpf A, Semiz K, Aydin F, deBivort B, Brembs B. Pain is so close to pleasure: the same dopamine neurons can mediate approach and avoidance in Drosophila. bioRxiv. 2021. p. 2021.10.04.463010. doi:10.1101/2021.10.04.463010

66. Klapoetke NC, Murata Y, Kim SS, Pulver SR, Birdsey-Benson A, Cho YK, et al. Independent optical excitation of distinct neural populations. Nat Methods. 2014;11: 338–346.

67. Nässel DR, Elekes K. Aminergic neurons in the brain of blowflies and Drosophila: dopamine- and tyrosine hydroxylase-immunoreactive neurons and their relationship with putative histaminergic neurons. Cell Tissue Res. 1992;267: 147–167.

68. Pfeiffer BD, Jenett A, Hammonds AS, Ngo T-TB, Misra S, Murphy C, et al. Tools for neuroanatomy and neurogenetics in Drosophila. Proc Natl Acad Sci U S A. 2008;105: 9715–9720.

69. Jenett A, Rubin GM, Ngo T-TB, Shepherd D, Murphy C, Dionne H, et al. A GAL4-driver line resource for Drosophila neurobiology. Cell Rep. 2012;2: 991–1001.

70. Perisse E, Burke C, Huetteroth W, Waddell S. Shocking revelations and saccharin sweetness in the study of Drosophila olfactory memory. Curr Biol. 2013;23: R752–63.

71. Ho J, Tumkaya T, Aryal S, Choi H, Claridge-Chang A. Moving beyond P values: data analysis with estimation graphics. Nat Methods. 2019 [cited 20 Jun 2019]. doi:10.1038/s41592-019-0470-3

72. Dubnau J, Grady L, Kitamoto T, Tully T. Disruption of neurotransmission in Drosophila mushroom body blocks retrieval but not acquisition of memory. Nature. 2001;411: 476–480.

73. McGuire SE, Le PT, Davis RL. The role of Drosophila mushroom body signaling in olfactory memory. Science. 2001;293: 1330–1333.

74. Govorunova EG, Sineshchekov OA, Janz R, Liu X, Spudich JL. Natural light-gated anion channels: A family of microbial rhodopsins for advanced optogenetics. Science. 2015;349: 647–650.

75. Mohammad F, Stewart JC, Ott S, Chlebikova K, Chua JY, Koh T-W, et al. Optogenetic inhibition of behavior with anion channelrhodopsins. Nat Methods. 2017. doi:10.1038/nmeth.4148

76. Liu C, Plaçais P-Y, Yamagata N, Pfeiffer BD, Aso Y, Friedrich AB, et al. A subset of dopamine neurons signals reward for odour memory in Drosophila. Nature. 2012;488: 512–516.

77. Dietzl G, Chen D, Schnorrer F, Su K-C, Barinova Y, Fellner M, et al. A genome-wide transgenic RNAi library for conditional gene inactivation in Drosophila. Nature. 2007;448: 151–156.

78. Molinoff PB, Axelrod J. Biochemistry of catecholamines. Annu Rev Biochem. 1971;40: 465–500.

79. Bainton RJ, Tsai LT, Singh CM, Moore MS, Neckameyer WS, Heberlein U. Dopamine modulates acute responses to cocaine, nicotine and ethanol in Drosophila. Curr Biol. 2000;10: 187–194.

80. Neckameyer WS. Multiple roles for dopamine in Drosophila development. Dev Biol. 1996;176: 209–219.

81. Takemura S-Y, Aso Y, Hige T, Wong A, Lu Z, Xu CS, et al. A connectome of a learning and memory center in the adult Drosophila brain. Elife. 2017;6. doi:10.7554/eLife.26975

82. Montague SA, Baker BS. Memory Elicited by Courtship Conditioning Requires Mushroom Body Neuronal Subsets Similar to Those Utilized in Appetitive Memory. PLoS One. 2016;11: e0164516.

83. Dag U, Lei Z, Le JQ, Wong A, Bushey D, Keleman K. Neuronal reactivation

during post-learning sleep consolidates long-term memory in Drosophila. Elife. 2019;8. doi:10.7554/eLife.42786

84. Handler A, Graham TGW, Cohn R, Morantte I, Siliciano AF, Zeng J, et al. Distinct Dopamine Receptor Pathways Underlie the Temporal Sensitivity of Associative Learning. Cell. 2019;178: 60–75.e19.

85. Jacob PF, Waddell S. Spaced Training Forms Complementary Long-Term Memories of Opposite Valence in Drosophila. Neuron. 2020. doi:10.1016/j.neuron.2020.03.013

86. Borenstein M, Hedges LV, Higgins JPT, Rothstein HR. Introduction to Meta-Analysis. Wiley; 2009.

87. Tumkaya T, Ott S, Claridge-Chang A. Systematic review of Drosophila short-term-memory genetics: Meta-analysis reveals robust reproducibility. Neurosci Biobehav Rev. 2018. doi:10.1016/j.neubiorev.2018.07.016

88. Tanaka NK, Tanimoto H, Ito K. Neuronal assemblies of the Drosophila mushroom body. J Comp Neurol. 2008;508: 711–755.

89. Chiang A-S, Lin C-Y, Chuang C-C, Chang H-M, Hsieh C-H, Yeh C-W, et al. Three-dimensional reconstruction of brain-wide wiring networks in Drosophila at single-cell resolution. Curr Biol. 2011;21: 1–11.

90. Owald D, Felsenberg J, Talbot CB, Das G, Perisse E, Huetteroth W, et al. Activity of defined mushroom body output neurons underlies learned olfactory behavior in Drosophila. Neuron. 2015;86: 417–427.

91. Simões JM, Levy JI, Zaharieva EE, Vinson LT, Zhao P, Alpert MH, et al. Robustness and plasticity in Drosophila heat avoidance. Nat Commun. 2021;12: 2044.

92. Li F, Lindsey JW, Marin EC, Otto N, Dreher M, Dempsey G, et al. The connectome of the adult Drosophila mushroom body provides insights into function. Elife. 2020;9. doi:10.7554/eLife.62576

93. Berry JA, Cervantes-Sandoval I, Chakraborty M, Davis RL. Sleep Facilitates Memory by Blocking Dopamine Neuron-Mediated Forgetting. Cell. 2015;161: 1656–1667.

94. Fuenzalida-Uribe N, Campusano JM. Unveiling the Dual Role of the Dopaminergic System on Locomotion and the Innate Value for an Aversive Olfactory Stimulus in Drosophila. Neuroscience. 2018;371: 433–444.

95. Berridge KC, Kringelbach ML. Pleasure systems in the brain. Neuron. 2015;86: 646–664.

96. Llinas RR. I of the Vortex: From Neurons to Self. MIT Press; 2001.

97. Yildizoglu T, Weislogel J-M, Mohammad F, Chan ES-Y, Assam PN, Claridge-Chang A. Estimating Information Processing in a Memory System: The Utility of Meta-analytic Methods for Genetics. PLoS Genet. 2015;11: e1005718.

98. Vogt K, Aso Y, Hige T, Knapek S, Ichinose T, Friedrich AB, et al. Direct neural pathways convey distinct visual information to Drosophila mushroom bodies. Elife. 2016;5. doi:10.7554/eLife.14009

99. Croset V, Treiber CD, Waddell S. Cellular diversity in the Drosophila midbrain revealed by single-cell transcriptomics. Elife. 2018;7. doi:10.7554/eLife.34550

100. Aguilar JI, Dunn M, Mingote S, Karam CS, Farino ZJ, Sonders MS, et al. Neuronal Depolarization Drives Increased Dopamine Synaptic Vesicle Loading via VGLUT. Neuron. 2017;95: 1074–1088.e7.

101. Chuhma N, Zhang H, Masson J, Zhuang X, Sulzer D, Hen R, et al. Dopamine neurons mediate a fast excitatory signal via their glutamatergic synapses. J Neurosci. 2004;24: 972–981.

102. Stuber GD, Hnasko TS, Britt JP, Edwards RH, Bonci A. Dopaminergic terminals in the nucleus accumbens but not the dorsal striatum corelease glutamate. J Neurosci. 2010;30: 8229–8233.

103. Chuhma N, Mingote S, Moore H, Rayport S. Dopamine neurons control striatal cholinergic neurons via regionally heterogeneous dopamine and glutamate signaling. Neuron. 2014;81: 901–912.

104. Sabandal JM, Sabandal PR, Kim Y-C, Han K-A. Concerted Actions of Octopamine and Dopamine Receptors Drive Olfactory Learning. J Neurosci. 2020;40: 4240–4250.

105. Yang C-H, Shih M-FM, Chang C-C, Chiang M-H, Shih H-W, Tsai Y-L, et al. Additive Expression of Consolidated Memory through Drosophila Mushroom Body Subsets. PLoS Genet. 2016;12: e1006061.

106. Perkins LA, Holderbaum L, Tao R, Hu Y, Sopko R, McCall K, et al. The Transgenic RNAi Project at Harvard Medical School: Resources and Validation. Genetics. 2015;201: 843–852.

107. Cumming G, Calin-Jageman R. Introduction to the New Statistics: Estimation, Open Science, and Beyond. Routledge; 2016.

108. Dulcis D, Lippi G, Stark CJ, Do LH, Berg DK, Spitzer NC. Neurotransmitter Switching Regulated by miRNAs Controls Changes in Social Preference. Neuron. 2017;95: 1319–1333.e5.

109. Dulcis D, Jamshidi P, Leutgeb S, Spitzer NC. Neurotransmitter switching in the adult brain regulates behavior. Science. 2013;340: 449–453.

110. Meng D, Li H-Q, Deisseroth K, Leutgeb S, Spitzer NC. Neuronal activity regulates neurotransmitter switching in the adult brain following light-induced stress. Proc Natl Acad Sci U S A. 2018;115: 5064–5071.

111. Buck SA, Steinkellner T, Aslanoglou D, Villeneuve M, Bhatte SH, Childers VC, et al. VGLUT modulates sex differences in dopamine neuron vulnerability to age-related neurodegeneration. bioRxiv. 2020. p. 2020.11.11.379008.

doi:10.1101/2020.11.11.379008

112. Witten IB, Steinberg EE, Lee SY, Davidson TJ, Zalocusky KA, Brodsky M, et al. Recombinase-driver rat lines: tools, techniques, and optogenetic application to dopamine-mediated reinforcement. Neuron. 2011;72: 721–733.

113. Danjo T, Yoshimi K, Funabiki K, Yawata S, Nakanishi S. Aversive behavior induced by optogenetic inactivation of ventral tegmental area dopamine neurons is mediated by dopamine D2 receptors in the nucleus accumbens. Proc Natl Acad Sci U S A. 2014;111: 6455–6460.

114. Schultz W, Dayan P, Montague PR. A neural substrate of prediction and reward. Science. 1997;275: 1593–1599.

115. Kato S, Kaplan HS, Schrödel T, Skora S, Lindsay TH, Yemini E, et al. Global brain dynamics embed the motor command sequence of Caenorhabditis elegans. Cell. 2015;163: 656–669.

116. Temasek Life Sciences Laboratories. Recipe for Drosophila media. In: Zenodo [Internet]. 28 Feb 2018. doi:10.5281/zenodo.1185451

117. Jung Y, Kennedy A, Chiu H, Mohammad F, Claridge-Chang A, Anderson DJ. Neurons that Function within an Integrator to Promote a Persistent Behavioral State in Drosophila. Neuron. 2020;105: 322–333.e5.

118. Zars T, Fischer M, Schulz R, Heisenberg M. Localization of a short-term memory in Drosophila. Science. 2000;288: 672–675.

119. Pitman JL, Huetteroth W, Burke CJ, Krashes MJ, Lai S-L, Lee T, et al. A pair of inhibitory neurons are required to sustain labile memory in the Drosophila mushroom body. Curr Biol. 2011;21: 855–861.

120. Kan L, Ott S, Joseph B, Park ES, Dai W, Kleiner RE, et al. A neural m6A/Ythdf pathway is required for learning and memory in Drosophila. Nat Commun. 2021;12: 1458.

121. Tully T, Quinn WG. Classical conditioning and retention in normal and mutant Drosophila melanogaster. J Comp Physiol A. 1985;157: 263–277.

122. DiCiccio TJ, Efron B. Bootstrap Confidence Intervals. Stat Sci. 1996;11: 189–228.

123. Altman D, Machin D, Bryant T, Gardner S. Statistics with confidence: confidence interval and statistical guidelines. Bristol: BMJ Books. 2000.

124. Efron B, Tibshirani RJ. An Introduction to the Bootstrap. CRC Press; 1994.

Supplemental information for

A dopaminergic memory circuit drives acute valence via multiple neurotransmitters

Farhan Mohammad [1, 5, *], Yishan Mai [1, *], Joses Ho [2], Xianyuan Zhang [3], Stanislav Ott [1], James Charles Stewart [2], & Adam Claridge-Chang [1, 2, 4, 6]

1. Program in Neuroscience and Behavioural Disorders, Duke-NUS Medical School, Singapore.
2. Institute for Molecular and Cell Biology, A*STAR, Singapore.
3. Department of Pharmacology, National University of Singapore, Singapore.
4. Department of Physiology, National University of Singapore, Singapore.
5. Division of Biological and Biomedical Sciences, College of Health & Life Sciences, Hamad Bin Khalifa University, Qatar.
6. Correspondence: claridge-chang.adam@duke-nus.edu.sg

* Equal contribution

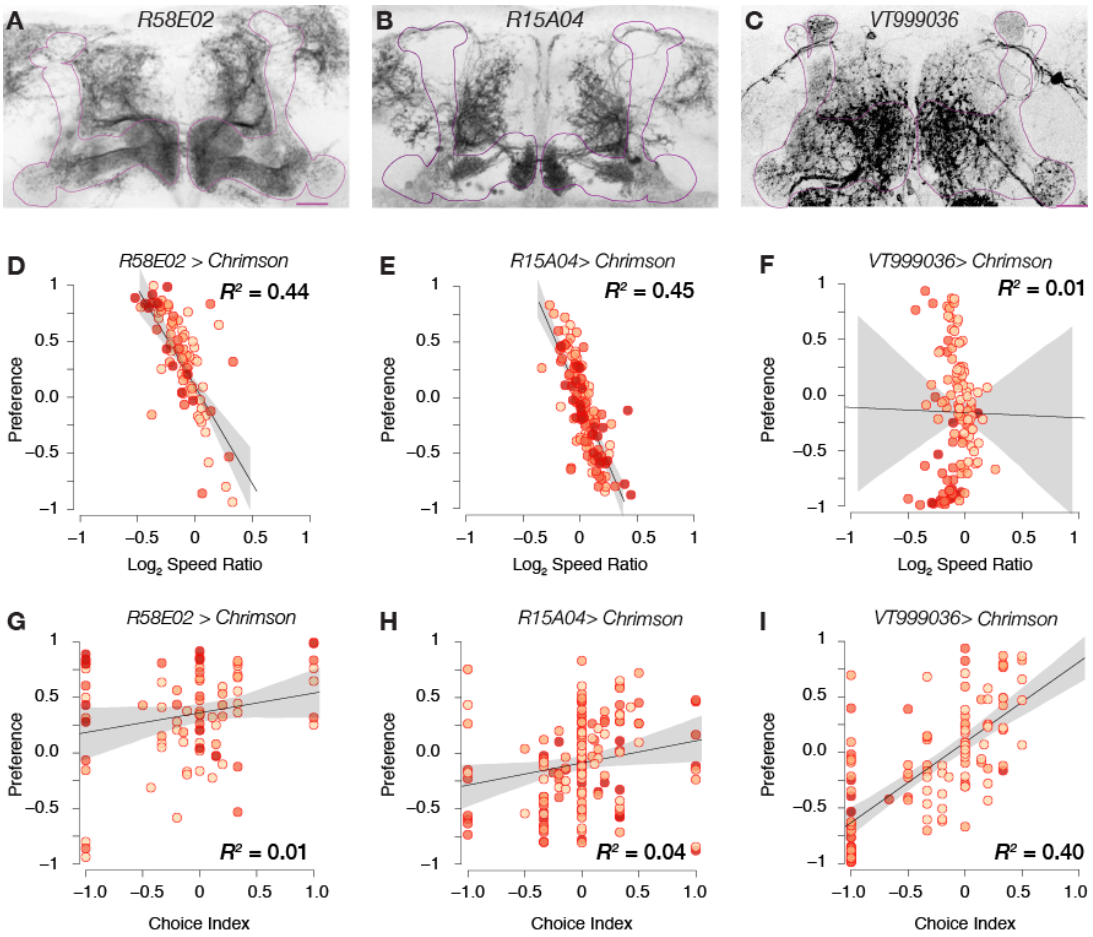

Figure S1. Relationship exploration between valence and locomotor modes.

A-C. The mushroom-body neuropil is innervated by *R58E02*, *R15A04* and *VT999036* in a variety of zonal patterns. The neuropil was outlined from a neuropil counterstain (see Methods for details). Scale bar represents 20 µm.

D. Scatter plots and linear regression of *R58E02>Chr* preference indices (PIs) with their light/dark $\log_2$ speed ratios revealed that the two metrics have a negative relationship; R^2_{adj} = 0.44 (95 CI, 0.24, 0.62, $P = 2.9 \times 10^{-12}$). N = 86. Each point indicates the $\log_2$ speed ratio and PI of a single fly. Flies were assayed at 1.3, 5, 22, and 72 µW/mm^2.

E. There is an inverse relationship between *R15A04>Chr* PIs and speed ratios; R^2_{adj} = 0.45 (95 CI, 0.3, 0.6, $P = 1.2 \times 10^{-20}$).

F. A relationship between PI and speed ratios was absent in *VT999036>Chr* flies; R^2_{adj} = 0.01 (95 CI, 0.00, 0.07, $P = 3.4 \times 10^{-1}$).

G-I. Scatter plots of the relationships between PI and a choice index. PI and choice were unrelated in the two DAN lines. Choice and PI were related in *VT999036*: R^2_{adj} = 0.40 (95 CI, 0.23, 0.54, $P = 2.7 \times 10^{-13}$). Each point indicates metrics for a single fly. Flies were screened at 1.3, 5, 22, and 72 µW/mm^2.

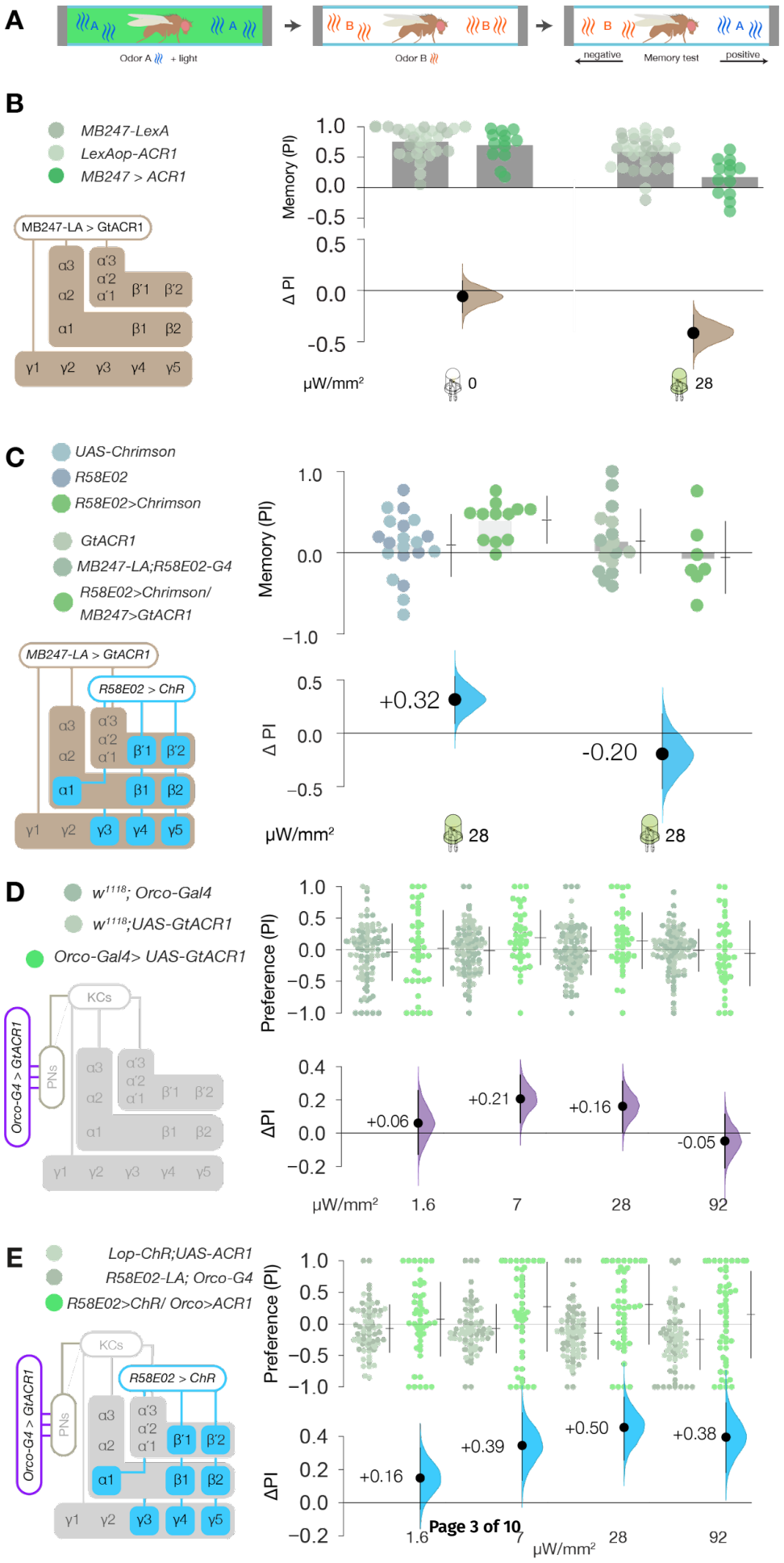
A
Odor A + light
Odor B
negative
Memory test
positive
B
MB247-LexA
LexAop-ACR1
MB247 > ACR1
MB247-LA > GtACR1
Memory (PI)
Δ PI
μW/mm²
0
28
C
UAS-Chrimson
R58E02
R58E02>Chrimson
GtACR1
MB247-LA;R58E02-G4
R58E02>Chrimson/
MB247>GtACR1
MB247-LA > GtACR1
R58E02 > ChR
Memory (PI)
Δ PI
+0.32
-0.20
μW/mm²
28
28
D
w1118; Orco-Gal4
w1118;UAS-GtACR1
Orco-Gal4> UAS-GtACR1
Orco-G4 > GtACR1
KCs
PNs
Preference (PI)
ΔPI
+0.06
+0.21
+0.16
-0.05
μW/mm²
1.6
7
28
92
E
Lop-ChR;UAS-ACR1
R58E02-LA; Orco-G4
R58E02>ChR/ Orco>ACR1
Orco-G4 > GtACR1
KCs
R58E02 > ChR
PNs
Preference (PI)
ΔPI
+0.16
+0.39
+0.50
+0.38
1.6
7
28
92
μW/mm²

Figure S2. Memory depends on olfactory system function, optogenetic PAM DAN valence does not.

A. An optogenetic olfactory conditioning protocol: two odors are presented to flies in sequence, one with light; then, the two odors are presented in different arms of the chamber to test the conditioned preference (see Methods for details).

B. Relative to unilluminated controls, silencing the KCs with ACR1 actuation decreases aversive shock memory by 75.0% [95CI -44%, -104%].

C. Green-light DAN activation paired with odor instructs an attractive olfactory memory in *R58E02>Chr* flies. Green light induces aversive memory formation in *R58E02>Chr/ MB247>ACR1* flies. The difference attributable to ACR1 inhibition corresponds to a performance reduction of –120% [95CI –200%, –24%]. Sample sizes: $N_{experiments}$ = 6, 6, 6; N_{flies} = 144 per genotype.

D. *Orco>ACR1* flies display moderate attraction to green light at two intermediate intensities (5 and 22 μW/mm^2), but not at 72 μW/mm^2.

E. Simultaneous inhibition of the olfactory receptor neurons has no impact on attraction to PAM DAN activation. At 92 μW/mm^2 the ΔPI was +0.38 [95CI +0.17, +0.6], P = 0.002.

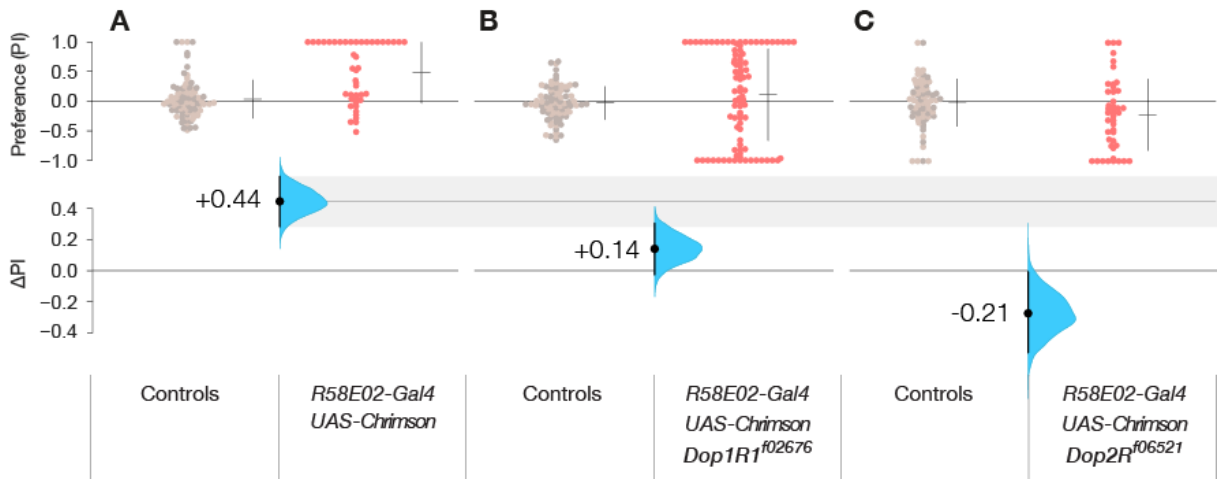

Figure S3. The Dopamine 2 Receptor is the major mediator of PAM DAN attraction.

A. Control *R58E02>Chr* flies are attracted to red light. ΔPI = +0.45 [95CI +0.28, +0.61], P = 0.06.

B. Loss of Dop1R1 (*Dop1R1*^{f02676}) reduces opto-attraction in *R58E02>Chr* flies. ΔPI = +0.14 [95CI -0.03, +0.31], $P = 9.6 \times 10^{-9}$.

C. Loss of Dop2R2 (*Dop2R2*^{f06521} null) reverses opto-attraction in *R58E02>Chr* flies to aversion. ΔPI = -0.21 [95CI -0.4, -0.01], P = 0.02.

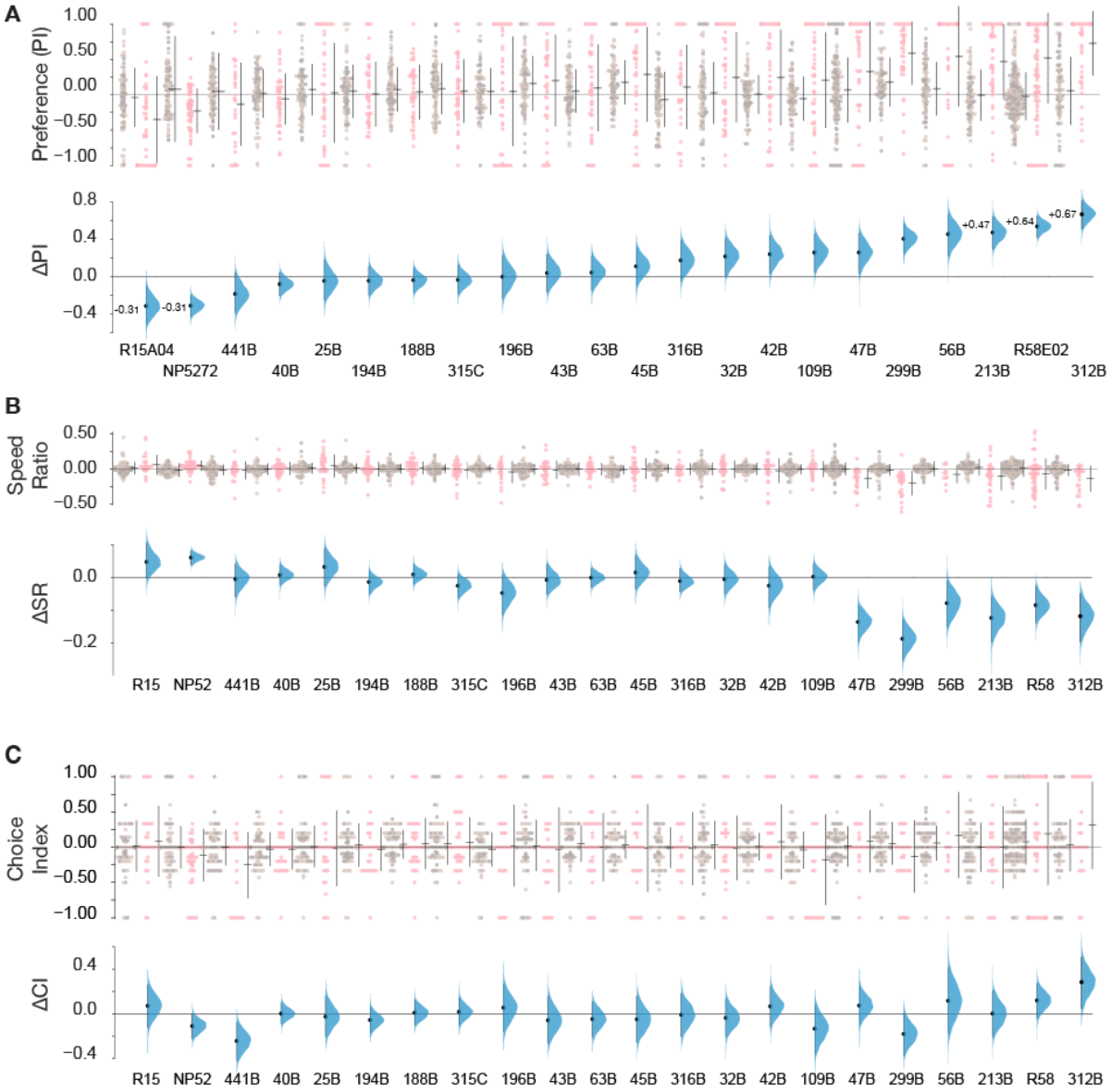

Figure S4. Screening DAN drivers for valence, speed and choice effects

A. The preference and valence metrics of 22 DAN split-Gal4 drivers expressing CsChrimson (light red) and controls (grays). Upper panel shows observed PI values, lower panel shows optogenetic valence effect sizes (ΔPI). The data are ordered by valence. All illumination was 70 µW/mm2.

B–C. Speed ratios and choice indices of the transgenic lines; the lower panels show optogenetic effect sizes (Δspeed ratio, Δchoice).

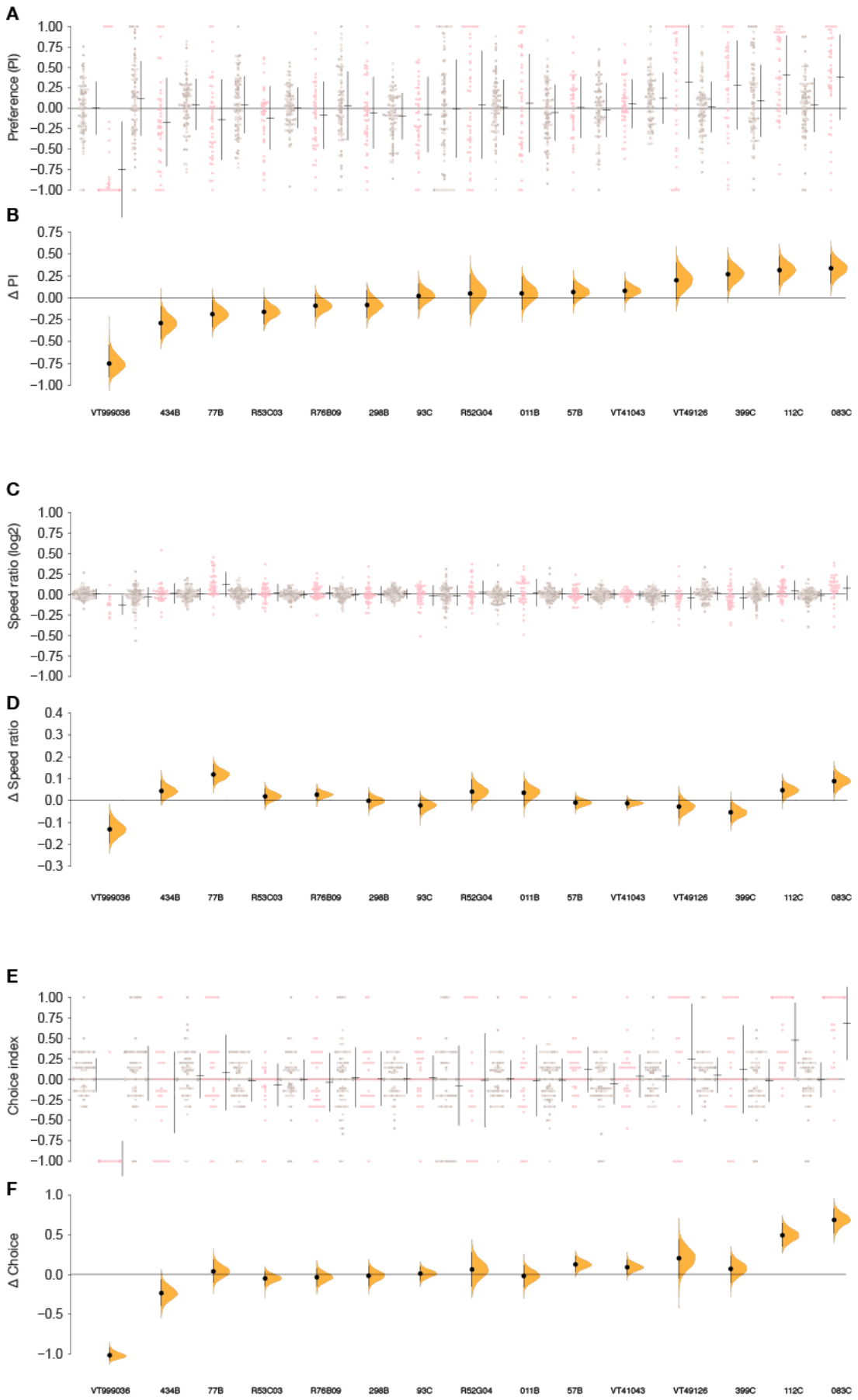
A
Preference (PI)
1.00
0.75
0.50
0.25
0.00
−0.25
−0.50
−0.75
−1.00
B
Δ PI
0.75
0.50
0.25
0.00
−0.25
−0.50
−0.75
−1.00
VT999036
434B
77B
R53C03
R76B09
298B
93C
R52G04
011B
57B
VT41043
VT49126
399C
112C
083C
C
Speed ratio (log2)
1.00
0.75
0.50
0.25
0.00
−0.25
−0.50
−0.75
−1.00
D
Δ Speed ratio
0.4
0.3
0.2
0.1
0.0
−0.1
−0.2
−0.3
VT999036
434B
77B
R53C03
R76B09
298B
93C
R52G04
011B
57B
VT41043
VT49126
399C
112C
083C
E
Choice index
1.00
0.75
0.50
0.25
0.00
−0.25
−0.50
−0.75
−1.00
F
Δ Choice
1.0
0.5
0.0
−0.5
−1.0
VT999036
434B
77B
R53C03
R76B09
298B
93C
R52G04
011B
57B
VT41043
VT49126
399C
112C
083C

Figure S5. Screening MBON drivers identified select lines that elicit valence.

A. The preferences and valence metrics of MBON drivers expressing CsChrimson. The upper panel shows the observed PI values; the lower panel shows optogenetic valence effect sizes (ΔPI). The data are ordered by valence. Illumination at 70 μW/mm^2.

B–C. Speed ratios and choice indices of the transgenic lines; the lower panels show optogenetic effect sizes (Δspeed ratio, Δchoice).

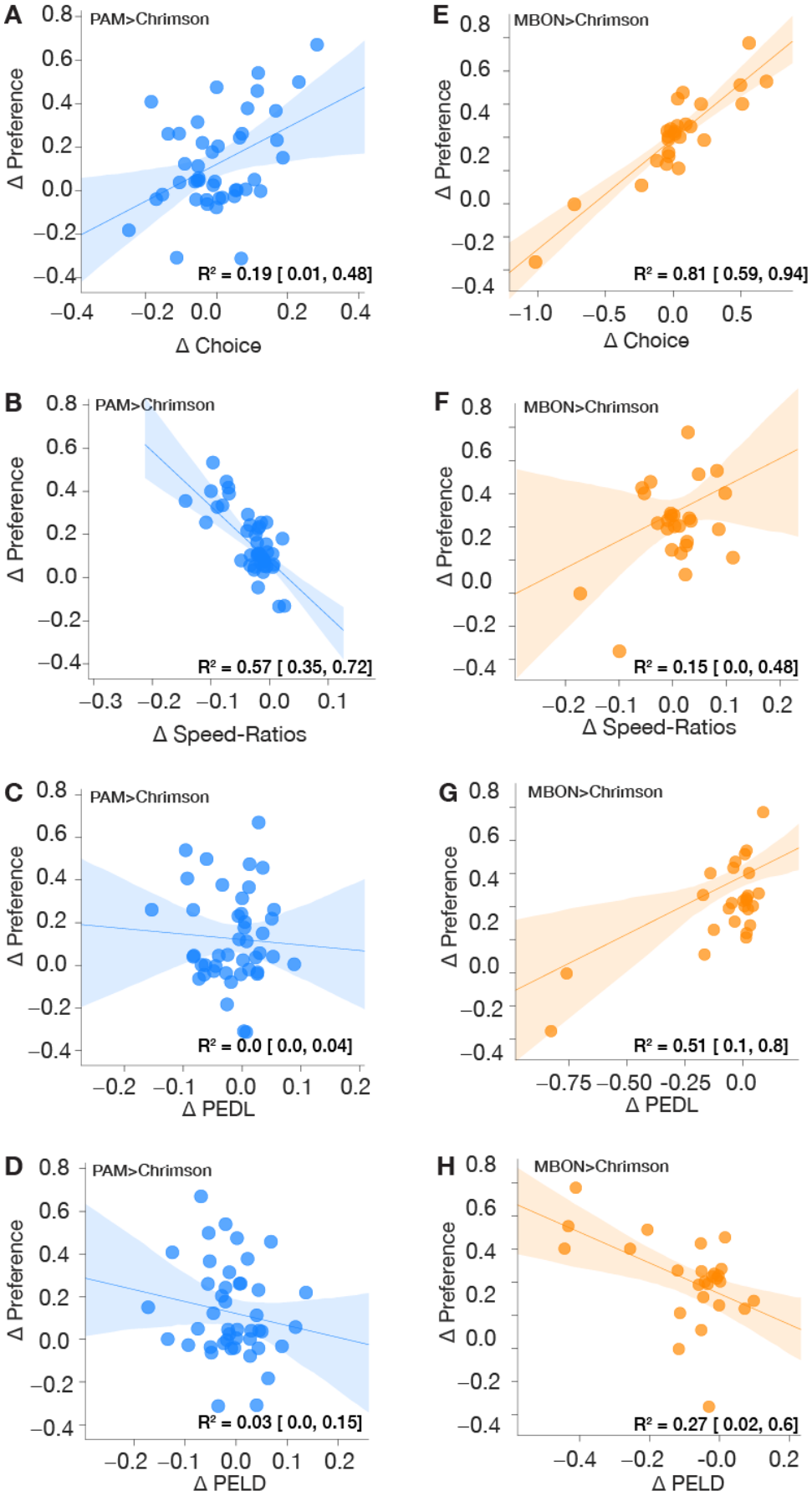
A
PAM>Chrimson
Δ Preference
Δ Choice
R² = 0.19 [0.01, 0.48]
E
MBON>Chrimson
Δ Preference
Δ Choice
R² = 0.81 [0.59, 0.94]
B
PAM>Chrimson
Δ Preference
Δ Speed-Ratios
R² = 0.57 [0.35, 0.72]
F
MBON>Chrimson
Δ Preference
Δ Speed-Ratios
R² = 0.15 [0.0, 0.48]
C
PAM>Chrimson
Δ Preference
Δ PEDL
R² = 0.0 [0.0, 0.04]
G
MBON>Chrimson
Δ Preference
Δ PEDL
R² = 0.51 [0.1, 0.8]
D
PAM>Chrimson
Δ Preference
Δ PELD
R² = 0.03 [0.0, 0.15]
H
MBON>Chrimson
Δ Preference
Δ PELD
R² = 0.27 [0.02, 0.6]

Figure S6. Regression analyses of DAN and MBON drivers.

A. Scatter plot showing the relationship between optogenetic valence and choice effects (ΔPI and Δchoice) of DAN driver lines from Fig. S4. Each point indicates the two optogenetic effects for a single DAN driver. The data are obtained from the two bright illumination intensities (22 and 70 μW/mm^2).

B–D. Scatter plots relating valence with Δspeed ratio, Δproportion of dark→light exits (ΔPEDL) and Δproportion of dark→light exits (ΔPELD) in the DAN lines.

E–H. Scatter plots relating valence to Δchoice, Δspeed ratio, Δproportion of dark→light exits (ΔPEDL) and Δproportion of dark→light exits (ΔPELD) for the MBON lines from Fig. S5. The data are obtained from the two bright illumination intensities (22 and 70 μW/mm^2).

Table S1. Detailed genotypes and effect sizes

Genotypes and effect sizes of experiments in the main figures. Semicolons indicate different chromosomes, commas indicate different transgenes. Split-Gal4 compound drivers (each a pair of transgenes_ are indicated with plus signs before the driver name. For full compound genotypes, please refer to this site.

Movie S1. *R58E02>Chr* flies walk slower in light

Video of a 91-s-duration OSAR experiment. *R58E02>Chr* flies slow or stop upon entering the light. The video is slowed by 0.7×. Optogenetic light is turned on at t = 22 s and off at t= 106 s (video time). The light-border pattern was superimposed on the video (see Methods for details).

Movie S2. *VT999036>Chr* flies avoid light

VT999036>Chr flies avoid light using reversal and turning maneuvers. Timing is identical to Movie S1.

Movie S3. *R58E02-LexA>LexAOP-Chr/MBON-Gal4>Dop2R-RNAi* flies avoid light

In a Dop2R knockdown background, *R58E02>Chr* flies avoid light using reversal and turning maneuvers. Timing is identical to Movie S1.